Univerzita Karlova v Praze
Matematicko-fyzikální fakulta

DIPLOMOVÁ PRÁCE

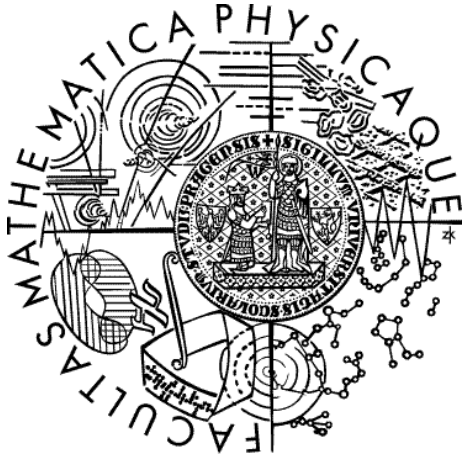

Václav Březina

Spektroskopické a teoretické studium supramolekulárních komplexů symetrických porfyrinů s chirálními guesty

Katedra makromolekulární fyziky

Vedoucí diplomové práce: doc. RNDr. Lenka Hanyková Dr.

Studijní program: Fyzika

Studijní obor: Fyzika kondenzovaných soustav a materiálů

Praha 2014

Charles University in Prague
Faculty of Mathematics and Physics

MASTER THESIS

Václav Březina

Spectroscopic and theoretical study of supramolecular complexes of symmetric porphyrins with chiral guests

Department of Macromolecular Physics

Supervisor of the master thesis: doc. RNDr. Lenka Hanyková Dr.

Study programme: Physics

Specialization: Physics of Condensed Matter and Materials

Prague 2014

I would like to thank to my supervisor Lenka Hanyková for help with NMR measurements. Many thanks belong to Jan Labuta for help with NMR measurements, consultations of processing obtained data, interpretation of results and providing UV-vis titration data. I would also like to thank to both of them for revisions of text of this master thesis. Another thanks belong to Jaroslav Burda for consultations of quantum chemistry computations and to Hana Kouřilová for help with NMR measurements and preparation of samples. I am also grateful to National Institute for Material Science, Tsukuba, Japan for providing samples.

Access to computing and storage facilities owned by parties and projects contributing to the National Grid Infrastructure MetaCentrum, provided under the programme "Projects of Large Infrastructure for Research, Development, and Innovations" (LM2010005), is greatly appreciated.

I declare that I carried out this master thesis independently, and only with the cited sources, literature and other professional sources.

I understand that my work relates to the rights and obligations under the Act No. 121/2000 Coll., the Copyright Act, as amended, in particular the fact that the Charles University in Prague has the right to conclude a license agreement on the use of this work as a school work pursuant to Section 60 paragraph 1 of the Copyright Act.

In ..... date ..... signature of the author

Název práce: Spektroskopické a teoretické studium supramolekulárních komplexů symetrických porfyrinů s chirálními guesty
Autor: Václav Březina
Katedra: Katedra makromolekulární fyziky
Vedoucí diplomové práce: doc. RNDr. Lenka Hanyková Dr., Katedra makromolekulární fyziky

Abstrakt: Některé typy porfyrinů můžou být použity jako achirální detektory při určování enantiomerního přebytku chirální látky. Porfyriny mohou tvořit komplex s chirálními organickými molekulami, které indukují neekvivalenci některých protonů v původně symetrickém porfyrinu. To má za následek rozštěpení příslušných signálů v NMR spektru, které závisí lineárně na enantiomerním přebytku chirální molekuly. V této práci jsme zkoumali komplex di-brombenzylovaného oxoporfyrinu s chirální kafrsulfonovou kyselinou. Z NMR titrace byla určena asociační konstanta $K \approx 5 \times 10^4$ l/mol a stechiometrie komplexu 1:1. Potvrdili jsme lineární závislost rozštěpení signálu β-protonu porfyrinu na enantiomerním přebytku. Nízkoteplotní měření prokázala existenci dvou různých konformací komplexu v přibližném poměru 0.7:0.3 (při -60 °C). Kvantově-mechanické výpočty metodou DFT za použití BLYP/3-21G* ukázaly rovněž dvě konformace v zastoupení 0.79:0.21. Metodou GIAO/PBE1PBE/6-31G(2df,2pd) byly vypočteny chemické posuny vypočtených struktur a porovnány s experimentálními hodnotami.
Klíčová slova: porfyrin, chiralita, spektroskopie nukleární magnetické rezonance (NMR), teorie funkcionálu hustoty (DFT)

Title: Spectroscopic and theoretical study of supramolecular complexes of symmetric porphyrins with chiral guests
Author: Václav Březina
Department: Department of Macromolecular Physics
Supervisor: doc. RNDr. Lenka Hanyková Dr., Department of Macromolecular Physics

Abstract: Certain types of porphyrins can be used as achiral agent for determination of enantiomeric excess (*ee*) of chiral molecules. Particular organic chiral molecule (guest) and porphyrin (host) form host-guest complex while inducing nonequivalency of particular proton resonances in symmetrical host. It causes splitting of NMR signals linearly dependent on *ee* of guest. In this work we investigated complexation of di-brombenzylated oxoporphyrin with chiral camphorsulfonic acid. NMR titration revealed that they form complex with 1:1 stoichiometry with association constant $K \approx 5 \times 10^4$ l/mol. We confirmed linear dependence of splitting of host β-protons on *ee* of guest. Low temperature measurements revealed two conformations of host-guest complex with population around 0.7:0.3 (at -60 °C). DFT quantum mechanical computations at BLYP/3-21G* level revealed also two conformations with population 0.79:0.21. NMR shifts were computed on this geometries with method GIAO/PBE1PBE/6-31G(2df,2pd) and compared to experimental values.
Keywords: porphyrin, chirality, nuclear magnetic resonance (NMR) spectroscopy, density functional theory (DFT)

Contents

Preface

Chiral molecules exists in two forms that are mirror images to each other but are not superimposable. This two forms are called enantiomers. Their difference has no influence on reactions with achiral molecules. However, if two chiral molecules react, the result depends on their particular enantiomeric form. Reactions between chiral molecules are very important in biological systems. Therefore determination of enantiomeric purity is important in drug design. Many ways of determining enantiomeric purity exist, however, many of them are based on reaction of the analyte with chiral agent. Recently, new method of determination of enantiomeric purity with *achiral* porphyrin agents via nuclear magnetic resonance spectroscopy was introduced.

Chapter 1

Introduction

1.1 Nuclear magnetic resonance

1.1.1 Basics

Nuclear magnetic resonance (NMR) spectroscopy ([1], [2]) is method detecting nuclei with nonzero magnetic dipole moment. Magnetic dipole moment $\vec{\mu}$ is directly proportional to nuclear spin $\vec{I}$:

$$\vec{\mu} = \gamma\hbar\vec{I}, \tag{1.1}$$

where γ is magnetogyric ratio. Therefore, detectable are nuclei with nonzero spin[1]. Signal of particular type of nucleus is proportional to size of its γ, I and abundance of its particular nuclide in the sample.

During measurement, the sample is placed into large constant external magnetic field $\vec{B_0}$ parallel with z-axis. Therefore, in the case of spin 1/2 ground state energy level of nuclei splits into two levels corresponding to the magnetic quantum number I_z. Energy of magnetic dipole in magnetic field $\vec{B_0}$ is

$$E_{mag\,dip} = -\vec{\mu}.\vec{B_0}, \tag{1.2}$$

thus splitting of energy levels has value:

$$\Delta E = \gamma B_0 \hbar = \omega_0 \hbar\,, \tag{1.3}$$

where ω_0 is Larmor frequency. Constant magnetic field induces nonzero nuclear magnetization because after splitting according to equation 1.2, the lower level including nuclei with $\langle I_z\rangle > 0$ is more populated then the higher level including nuclei with $\langle I_z\rangle < 0$ due to Boltzmann factor $\exp(-\Delta E/k_B T)$. In addition particular nuclear magnetic moments rotate around z-axis. Signal from the sample is detected by receiver coil in the xy plane. However, in this case no signal current in receiver coil is induced because particular dipoles are incoherent and create no macroscopic magnetization.

In order to receive signal from sample, it is irradiated with electromagnetic field of reference phase ϕ_{ref} and reference frequency ω_{ref} close to ω_0 so that weak magnetic radiofrequency field parallel with x-axis $\vec{B}_{RF}(t) = \vec{B}_{RF,\,0}\cos(\omega_{ref}t + \phi_{ref})$

[1] Nonzero spin have all nuclei except these with both even atomic number and even nucleon number.

is applied[2,3]. After applying radiofrequency field, particular dipoles start rotating coherently, create macroscopic magnetisation and in the receiver coil signal is induced.

Now, instead of laboratory frame xyz let us consider rotating frame x'y'z' that rotates around z-axis with reference frequency ω_{ref}. Irradiation of sample is in the form of radiofrequency pulses of duration τ (It means that radiofrequency field has the form[4] $\vec{B}_{RF}(t) = \vec{B}_{RF,0}\cos(\omega_{ref}t+\phi_{ref})\chi(t)_{\langle 0,\tau\rangle}$.). If we are interested only in macroscopic magnetization, before applying the pulse it is constant and parallel to z'-axis, Figure 1.1a. During applying the radiofrequency pulse magnetization will rotate about so called nutation axis placed in the x'y' plane with angular frequency ω_{nut}. This moving is denoted nutation and for ω_{nut} it holds:

$$\omega_{nut} = |\frac{1}{2}\gamma B_{RF,0}|. \tag{1.4}$$

So after application of pulse with duration τ magnetization deflects from z'-axis by angle $\omega_{nut}\,\tau$, Figure 1.1b. Orientation of nutation axis in the x'y' plane depends on pulse reference phase ϕ_{ref}. Pulses are denoted in this manner: $(\omega_{nut}\tau)_{nutation\,axis}$.

After deflection from z'-axis, magnetization begins to rotate around z'-axis with frequency $\omega_0 - \omega_{ref}$, Figure 1.1c. It means that macroscopic magnetization rotates in the laboratory frame with the Larmor frequency and induces signal in the receiver coil.

After ending of pulse, magnetization $\vec{M}$ gradually returns to its equilibrium position in direction of z-axis. This phenomenon reads relaxation. It is phenomenologically described with two relaxation times: T_1 - longitudinal relaxation of z-component M_z and T_2 - transverse relaxation of x, y-component M_x and M_y.

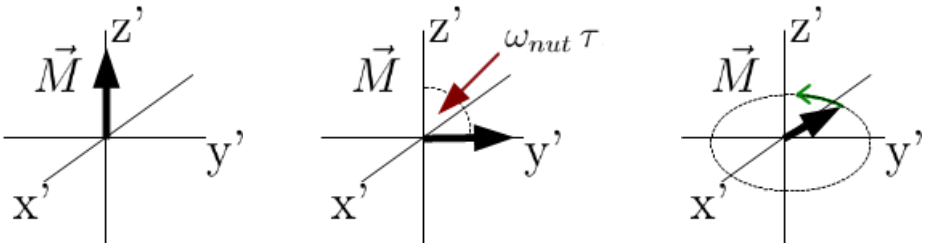

(a) (b) (c)

Figure 1.1: Ilustration: evolution of magnetization before (a), during (b) and after (c) application of $(\pi/2)_{-x}$ radiofrequency pulse.

Chemical shift

Electrons significantly influence NMR spectrum. In the presence of magnetic field B_0 they induce shielding field of opposite direction[5] that is proportional to B_0:

$$\vec{B}_{shield} = -\sigma\vec{B}_0, \tag{1.5}$$

[2]In presence of widely used magnetic field B_0 strengths Larmor frequency is in the radiofrequency region (order 100 MHz).

[3]Strength of magnetic field of used spectrometers is often denoted in MHz, it means Larmor frequency of hydrogen nucleus in the particular constant magnetic field B_0.

[4]$\chi(x)_{\langle a,\,b\rangle}$ is characteristic function of interval $\langle a,\,b\rangle$, equals zero outside and unity inside this interval.

[5]In case of diamagnetic elements.

σ is shielding constant. Shielding field sums with the field B_0 and they create local field B_{loc} that influences Larmor frequency of the particular nucleus:

$$\omega_0 = \gamma B_{loc} = \gamma(1-\sigma)B_0. \tag{1.6}$$

This phenomenon is called chemical shift. It depends on orientation of particular molecule with respect to the external magnetic field $\vec{B}_0$ but in the case of liquid sample chemical shifts becomes scalar quantity (due to motional averaging)

For experimental purposes, spectra are not depicted as functions of Larmor frequency because it depends on spectrometer magnetic field B_0. Instead, resonance frequencies (chemical shifts) are expressed in relative units. In order to allow easy calibrating of spectra, chemical shift δ defined as

$$\delta \equiv \frac{\omega_0 - \omega_{standard}}{\omega_{standard}}.10^6, \tag{1.7}$$

where $\omega_{standard}$ is Larmor frequency of chemically stable substance (standard) which does not have influence on investigated spectrum. Widely used standard is tetramethylsilan (TMS). Unit of chemical shift is ppm (parts per milion) because of the factor 10^6.

J-coupling

Nuclear spins of the same molecule can interact. Direct interaction of their magnetic dipoles is averaged out in liquid samples. However, nuclear magnetic dipoles interact also through the ambient electrons - typically through one up to four chemical bonds. This interaction is called J-coupling and its strength is described by the constant J. J-coupling is expressed in NMR spectrum by splitting both peaks of interacting nuclei into two or more peaks. For the number of split peaks m it holds: $m = 2nI + 1$ where n is number of equivalent nuclei with spin I they are J-coupled with the split resonance. For example consider molecule of ethyl bromide CH_3-CH_2-Br and its proton NMR spectrum, Figure 1.2. In this molecule only H nuclei with spin $I = 1/2$ are present. Note that methyl group rotates and chemical shifts of all three protons are averaged. Spectrum of methyl group consists of three peaks because in presence of external magnetic field the J-coupled methylene protons can be in three different spin states: (1/2,1/2), (-1/2,-1/2) and (1/2,-1/2) which is the twice more probable state. Therefore, in the spectrum appear three methyl peaks ($m = 2 \times 2 \times 1/2 + 1 = 3$) and one of then is two times more intensive. Similar situation is in case of methylen peaks. They neighbour with $n = 3$ equivalent methyl protons thus they split into $m = 2 \times 3 \times 1/2 + 1 = 4$ peaks.

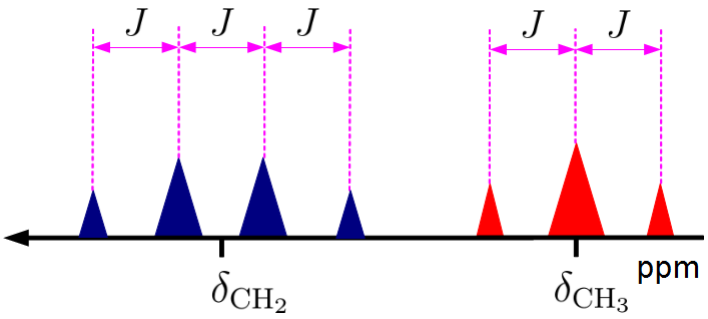

Figure 1.2: Ilustration of J-coupling effects on NMR spectrum.

1.1.2 Peak shapes

Quantum mechanics is needed for accurate description effects of radiofrequency pulses on spin systems. However, classical model of magnetzation vector in external magnetic field is also useful when we introduce phenomenological effects of longitudinal and transverse relaxation times T_1 and T_2. Equations describing behavior of magnetization vector are called Bloch equations:

$$\begin{aligned} \frac{\mathrm{d}M_x}{\mathrm{d}t} &= \gamma(\vec{M} \times \vec{B})_x - \frac{M_x}{T_2} \\ \frac{\mathrm{d}M_y}{\mathrm{d}t} &= \gamma(\vec{M} \times \vec{B})_y - \frac{M_y}{T_2} \\ \frac{\mathrm{d}M_z}{\mathrm{d}t} &= \gamma(\vec{M} \times \vec{B})_z - \frac{M_z - M_0}{T_1}, \end{aligned} \tag{1.8}$$

where $\vec{M}_0$ is equilibrium magnetization and $\vec{B} = \vec{B}_0 + \vec{B}_{RF}$. Signal in the receiver depends on time derivation of $M_x(t)$. After aquisition Fourier transform is performed. Chemical shifts of particular nuclei and corresponding peak shapes do not depend only on chemical shifts of particular protons but also depend on another influences. In this work we need three different forms for peak shapes as discussed below.

Lorentzian peak shape

Lorentzian peak shape is the simplest. It originates from signal of one standalone nucleus which is not influenced by other nuclei and its ambient does not change and can be derived from the Bloch equations 1.8.

$$S(\delta) = \frac{I\gamma^2}{(\delta - \delta_0)^2 + \gamma^2}. \tag{1.9}$$

Parameter I denotes peak height, 2γ its FWHM[6] and δ_0 denotes position of peak maximum. Area of this peak equals $\pi\gamma I$. FWHM of Lorentzian peak shape depends on relaxation time T_2, exactly on T_2^* where also broadening due to inhomogeneities of magnetic field B_0, it holds FWHM $= 1/\mathrm{T}_2^*$.

[6]Full Width at Half Maximum

Chemical exchange

Dynamic processes in the sample cause that the closest environment of nuclei changes in time. Thus chemical shifts also change in time and it influences peak shapes. This phenomenon is called chemical exchange. Let us consider chemical exchange between two states A and B:

$$\mathrm{A} \underset{k_A}{\overset{k_B}{\rightleftharpoons}} \mathrm{B}$$

where k_A and k_B are corresponding rate constants. Effect of chemical exchange on magnetisation could be described by Bloch-McConnell equations:

$$\begin{aligned}
\frac{\mathrm{d}M_x^A}{\mathrm{d}t} &= \gamma(\vec{M}^A \times \vec{B})_x - \frac{M_x^A}{T_2^A} - k_B M_x^A + k_A M_x^B \\
\frac{\mathrm{d}M_y^A}{\mathrm{d}t} &= \gamma(\vec{M}^A \times \vec{B})_y - \frac{M_y^A}{T_2^A} - k_B M_y^A + k_A M_y^B \\
\frac{\mathrm{d}M_z^A}{\mathrm{d}t} &= \gamma(\vec{M}^A \times \vec{B})_z - \frac{M_z^A - M_0^A}{T_1^A} - k_B M_z^A + k_A M_z^B \\
\frac{\mathrm{d}M_x^B}{\mathrm{d}t} &= \gamma(\vec{M}^B \times \vec{B})_x - \frac{M_x^B}{T_2^B} - k_A M_x^B + k_B M_x^A \\
\frac{\mathrm{d}M_y^B}{\mathrm{d}t} &= \gamma(\vec{M}^B \times \vec{B})_y - \frac{M_y^B}{T_2^B} - k_A M_y^B + k_B M_y^A \\
\frac{\mathrm{d}M_z^B}{\mathrm{d}t} &= \gamma(\vec{M}^B \times \vec{B})_z - \frac{M_z^B - M_0^B}{T_1^B} - k_A M_z^B + k_B M_z^A \,, \qquad (1.10)
\end{aligned}$$

where $\vec{M}_{(0)}^{A,B}$ denote equilibrium magnetization of the particular states A, B.

Peak shapes under chemical exchange depend on rate constants k_A, k_B and difference in chemical shifts of particular states $\Delta\delta \equiv \delta_A - \delta_B$ (or correspondent Larmor frequency difference $\omega_A = \omega_B$). Consider symmetrical chemical exchange $k_A = k_B \equiv k$. Dependence of peak shapes on k is depicted in Figure 1.3. We distinguish three regimes:

1. Slow exchange

   occurs when $k \ll |\omega_A - \omega_B|/2$. Two Lorentzian shape-like resonances with shifts δ_A and δ_B are observed (red arrow in the Figure 1.3.).

2. Intermediate exchange

   occurs when $k \approx |\omega_A - \omega_B|/2$. In this case both peaks begin to broaden and coalesce to one broad peak when k reaches exactly the value $|\omega_A - \omega_B|/2$ (green arrow in the Figure 1.3.).

3. Fast exchange

   If $k \gg |\omega_A - \omega_B|/2$ only one sharp peak is observed. Its chemical shift is average of actual shifts δ_A and δ_B (blue arrow in the Figure 1.3.).

Let us denote R_A and R_B FWHMs of both peaks if the case without exchange ($k = 0$). Then peak shape of all three exchange regimes is described by the form:

$$S(\delta) = M\frac{AC + BD}{C^2 + D^2} \qquad (1.11)$$

where

$$\begin{aligned} A &= 4k + R_A + R_B \\ B &= 2\omega - \omega_A - \omega_B \\ C &= R_A R_B + k(R_A + R_B) - (\omega - \omega_A)(\omega - \omega_B) \\ D &= (\omega - \omega_A)(k + R_B) + (\omega - \omega_B)(k + R_A)\,. \end{aligned}$$

Units [rad/s] were used for chemical shifts ω. Relation to chemical shift δ in [ppm] units is given by this form:

$$\omega\,[\text{rad/s}] = \delta\,[\text{ppm}] \times 2\pi \times \text{spectrometer frequency}\,[\text{MHz}]\,. \tag{1.12}$$

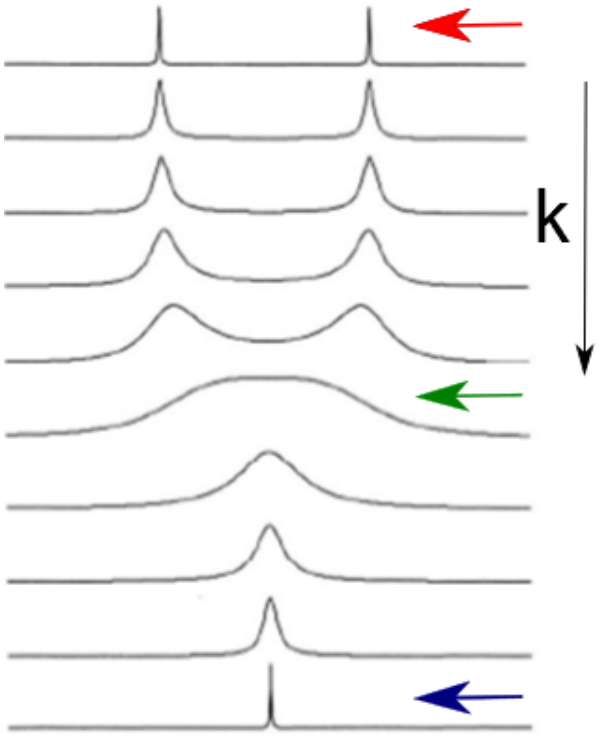

Figure 1.3: Peaks under chemical exchange for different values of k. Red, green and blue arrows denote slow, intermediate and fast exchange, respectively.

AB system

More complicated is system of two strongly interacting nuclei, it is denoted as AB system[7]. Interaction strength is dependent of size of J-coupling constant, strong interaction occurs under the condition $|\omega_A - \omega_B| \lesssim |\pi J|$. In this case not only splitting of corresponding peaks occurs but in addition intensity of outer peaks is lower then intensity of the inner peaks, see figure 1.4[8]. However, it is pure

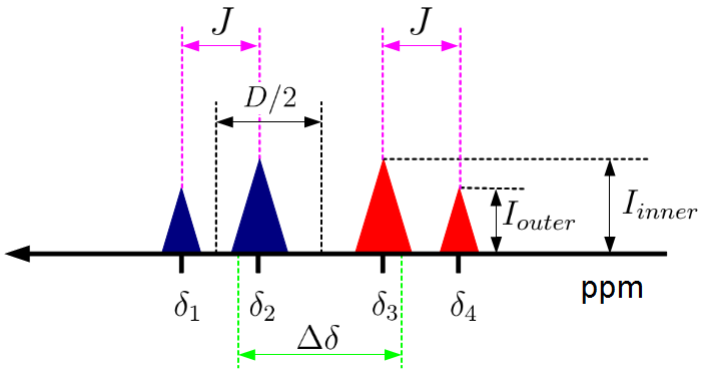

Figure 1.4: Observed peaks of homonuclear AB system.

quantum effect that cannot be derived from Bloch equations. All four peaks have Lorenzian shape and in the case of homonuclear AB system these equations hold:

$$\begin{aligned}
\delta_1 &= \frac{\delta_A + \delta_B}{2} + \frac{1}{2}(D + J) \\
\delta_2 &= \frac{\delta_A + \delta_B}{2} + \frac{1}{2}(D - J) \\
\delta_3 &= \frac{\delta_A + \delta_B}{2} - \frac{1}{2}(D - J) \\
\delta_4 &= \frac{\delta_A + \delta_B}{2} - \frac{1}{2}(D + J),
\end{aligned} \tag{1.13}$$

where $D = \sqrt{(\delta_A - \delta_B)^2 + J^2}$, δ_A and δ_B are actual chemical shifts of both nuclei. Intensities of inner and outer peaks satisfy this relation:

$$\frac{I_{inner}}{I_{outer}} = \frac{D + J}{D - J} \tag{1.14}$$

Peak splitting could be described with parameter $\Delta\delta \equiv \delta_A - \delta_B$. These relationships hold for this parameter:

$$\Delta\delta = \sqrt{D^2 - J^2} = \sqrt{(\delta_1 - \delta_4)(\delta_2 - \delta_3)}. \tag{1.15}$$

1.1.3 2D NMR experiments

Correlated spectroscopy (COSY) and Nuclear Overhauser effect spectroscopy (NOESY) are experiments in whose pulse sequence appears additional constant

[7] A and B are close in the alphabet thus it indicates strongly interacting nuclei. On the contrary, AX system denotes system of two weak interacting nuclei.

[8] It is sometimes called 'roof effect'.

parameter t_1, aquisition time is denoted t_2. More spectra with different parameter t_1 are obtained and then Fourier transform (FT) in both 'dimensions' t_1 and t_2 is performed (After FT both dimension are denoted F1 and F2). These spectra are depicted in this manner: x-axis - dimension F2 (usually better resolution), y-axis - dimension F1 and the peaks are viewed as points (horizontal cut through set of spectra). 2D spectra of COSY and NOESY contain diagonal peaks ($\delta(F1) = \delta(F2)$) and crosspeaks ($\delta(F1) \neq \delta(F2)$). Diagonal peaks contain no additional information compared to 1D spectrum. However, crosspeaks provide useful information. In the case of COSY (Figure 1.5) crosspeaks (denoted yellow) indicate J-coupling between corresponding resonances (J-coupling is nonnegligible up to four chemical bonds). In the case of NOESY crosspeaks prove spatial vicinity of corresponding nuclei (because of so called Overhauser effect).

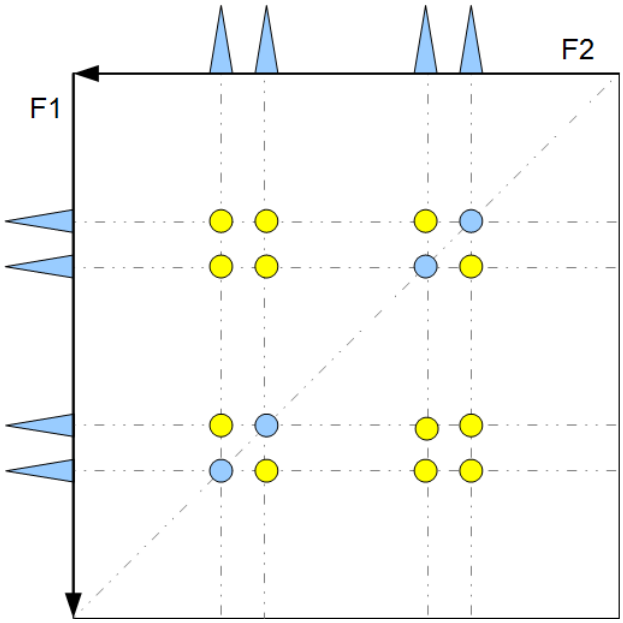

Figure 1.5: Schematic picture of COSY spectra of two J-coupled nuclei. Diagonal peaks are depicted blue, crosspeaks are denoted with yellow color.

1.2 Thermodynamics of complexation

1.2.1 Energy and population of conformers

Let us assume that host (**H**) and guest (**G**) molecules form host-guest complex (**HG**) with stoichiometry 1:1:

$$\mathbf{H} + \mathbf{G} \rightleftharpoons \mathbf{HG} \ .$$

Interaction energy of one host-guest complex molecule is defined as $\Delta E = E(\mathbf{HG}) - E(\mathbf{H}) - E(\mathbf{G})$, energies are ground states of quantum mechanics (QM) energy computations. However, statistical behavior of the whole ensemble of molecules must be taken into account. If we know energetic spectrum of particular molecule usage of canonical thermodynamics ensemble is appropriate. It uses these variables: temperature T, volume V and number of particles N.

Statistical sum of canonical ensemble is defined as:

$$Z(T,V,N) = \sum_{\substack{\text{possible}\\ \text{states}}} \exp\left(-\frac{E_i}{k_B T}\right) \tag{1.16}$$

where k_B is Boltzmann constant and E_i are energies of possible N-particle states. Now we have to find relation between N-particle and one-particle states (which are computed by QM). Assuming non-interacting particles (ideal gas) it holds:

$$Z(T,V,N) = Z(T,V,1)^N. \tag{1.17}$$

According to [3] one-particle statistical sum $Z(T,V,1)$ consists of four contributions:

1. contribution from translational molecular movement

$$Z_t(T,V,1) = \left(\frac{2\pi m k_B T}{h^2}\right)^{\frac{3}{2}} \frac{k_B T}{p},$$

   where p is pressure,

2. contribution from electronic motion, it is assumed that higher excited states are inaccessible

$$Z_e(T,V,1) = (2\tilde{S}+1)\exp\left(-\frac{\epsilon_0}{k_B T}\right),$$

   where $\tilde{S}$ is spin multiplicity and ϵ_0 is electronic energy of molecular ground state,

3. contribution from rotational motion

$$Z_r(T,V,1) = \frac{\sqrt{2 I_x I_y I_z}}{\sigma_r}\left(\frac{2 k_B T}{\hbar^2}\right)^{\frac{3}{2}},$$

   where $I_{x,y,z}$ are moments of inertia in the principal axes and σ_r is number of possible rotations that move the molecule around itself,

4. and vibrational contribution

$$Z_v(T,V,1) = \prod_{\substack{\text{possible}\\ \text{vibrational}\\ \text{modes}}} \frac{\exp\left(-\frac{\hbar\omega_i}{2k_B T}\right)}{1-\exp\left(-\frac{\hbar\omega_i}{k_B T}\right)},$$

   where ω_i are angular frequencies of vibrational modes.

Then one-particle statistical sum equals:

$$Z(T,V,1) = Z_t\, Z_e\, Z_r\, Z_v\,. \tag{1.18}$$

After constructing statistical sum $Z(T,V,N)$ entropy to one particle can be calculated as:

$$S = k_B + k_B \ln Z(T,V,N) + k_B T \left(\frac{\partial \ln Z(T,V,N)}{\partial T}\right)_V. \tag{1.19}$$

and energetic contributions to one particle can be obtained as:

$$E_{t,e,r,v} = k_B T^2 \left(\frac{\partial \ln Z_{t,e,r,v}(T,V,1)}{\partial T} \right)_V \tag{1.20}$$

Consequently Gibbs energy to one particle could be computed:

$$G = U + pV - TS = \epsilon_0 + E_t + E_e + E_r + E_v + k_B T - TS \tag{1.21}$$

where we used assumption of ideal gas and used its state equation $pV = k_B T$ and assumption that only ground state ϵ_0 is accessible, thus internal energy reads: $U = \epsilon_0 + E_t + E_e + E_r + E_v$.

Investigating of host-guest complex with QM computations can reveal more than one conformation. We are interested in their populations. Usage of canonical ensemble allows calculating population of i-th conformation with total energy E_i:

$$p_i = \exp\left(-\frac{E_i}{k_B T} \right) . \tag{1.22}$$

However, this approach does not include entropic effects thus population of possible states is computed as:

$$p_i = \exp\left(-\frac{G_i}{k_B T} \right) . \tag{1.23}$$

1.2.2 Equilibrium constant of association

Equilibrium association constant $K_{\mathbf{HG}}$ is an important quantity that describes strength of complexation. It is defined as:

$$K_{\mathbf{HG}} = \frac{[\mathbf{HG}]}{[\mathbf{H}][\mathbf{G}]}, \tag{1.24}$$

where $[\mathbf{H}]$ and $[\mathbf{G}]$ denote free host concentration (in mol/l) and $[\mathbf{HG}]$ is complex concentration.

We assume binding ratio 1:1. Denoting total concentrations

$$[\mathbf{H}]_{tot} \equiv [\mathbf{H}] + [\mathbf{HG}] \tag{1.25}$$

$$[\mathbf{G}]_{tot} \equiv [\mathbf{G}] + [\mathbf{HG}] \tag{1.26}$$

and taking them together with equation 1.24 we obtain 1:1 binding isotherm in that form[9]:

$$[\mathbf{HG}] = \frac{K_{\mathbf{HG}}([\mathbf{H}]_{tot} + [\mathbf{G}]_{tot}) + 1 - \sqrt{[K_{\mathbf{HG}}([\mathbf{H}]_{tot} - [\mathbf{G}]_{tot}) - 1]^2 + 4K_{\mathbf{HG}}[\mathbf{H}]_{tot}}}{2K_{\mathbf{HG}}} \tag{1.27}$$

or in equivalent form:

$$[\mathbf{HG}] = \frac{K_{\mathbf{HG}}([\mathbf{H}]_{tot} + [\mathbf{G}]_{tot}) + 1 - \sqrt{[K_{\mathbf{HG}}([\mathbf{H}]_{tot} + [\mathbf{G}]_{tot}) + 1]^2 - 4K_{\mathbf{HG}}[\mathbf{H}]_{tot}[\mathbf{G}]_{tot}}}{2K_{\mathbf{HG}}}. \tag{1.28}$$

[9] We have to solve one quadratic equation, we choose the right sign from the condition $[H] > 0$.

1.3 Density functional theory

Density functional theory (DFT) calculations [4] are not computationally expensive as post-Hartree-Fock methods although they also calculate with electron correlation.

Electron density of molecule is given by

$$\rho(\vec{r}) = N \sum_{\sigma_1=\pm 1/2} \int \mathrm{d}\tau_2 \mathrm{d}\tau_3 ... \mathrm{d}\tau_N |\psi(\vec{r}, \sigma_1, \vec{r}_2\sigma_2, ..., \vec{r}_N, \sigma_N)|^2 \tag{1.29}$$

where N is number of electrons and ψ is N-electron wavefunction. Integral of $\rho(\vec{r})$ over the whole space gives the number of electrons N. Basic fact that allows using DFT is theorem proved by Kohn and Hohenberg which says that ground state is fully described not only with wavefunction but also with electron density. Kohn and Hohenberg proved also relation that says ground state density ρ_g gives the minimum for functional of energy:

$$E[\rho] \geq E[\rho_g] \equiv E_g \,. \tag{1.30}$$

Energy functional can be written in the form:

$$E = T_0 + \int v(\vec{r})\rho(\vec{r})\mathrm{d}^3\vec{r} + J[\rho] + E_{xc}[\rho] \,. \tag{1.31}$$

The first term, kinetic energy of electrons cannot be easily expressed as function of ρ. It can be approximated by kinetic energy of N non-interacting particles described with so called Kohn-Sham orbitals ϕ_i (using atomic units):

$$T_0 = -\frac{1}{2} \sum_{i=1}^{N} \langle \phi_i | \Delta | \phi_i \rangle \ . \tag{1.32}$$

Second term describes interaction between electrons and nuclei,

$$v(\vec{r}) = \sum_A -\frac{Z_A}{|\vec{r} - \vec{r}_A|} \,. \tag{1.33}$$

Third term is self-interaction of the electron cloud itself:

$$J[\rho] = \frac{1}{2} \int \int \frac{\rho(\vec{r}_1)\rho(\vec{r}_2)}{|\vec{r}_1 - \vec{r}_2|} \,. \tag{1.34}$$

The last term describes exchange and correlation energy.

Minimum of this energy functional can be obtained by solving of Kohn-Sham equations:

$$\left(-\frac{1}{2} + v + v_{coul} + v_{xc} \right) \phi_i = \epsilon_i \phi_i \,, \tag{1.35}$$

where v_{coul} is coulombic potential describing coulombic interaction between nuclei and v_{xc} is exchange potential describing exchange and correlation energy of nuclei. Particular QM DFT methods consist in suggesting different forms of exchange and correlation part of the energy functional.

1.4 Porphyrins

1.4.1 Introduction

Term porphyrins comprises tetrapyrrole macrocycles and their derivatives. Basic tetrapyrrole structure is denoted as porphyrin or porphine. Porphine is perfectly planar because of sp2 hybridization of all its carbons. According to IUPAC [5] numbering of porphine carbons seems like in the picture 1.6a. However, it is common denoting carbon and their appended hydrogens as *meso* (sites 5, 10, 15, 20) and β (sites 2, 3, 7, 8, 12, 13, 17, 18). Another tetrapyrrole macrocycle is called porphyrinogen (Figure 1.6b). It differs from porphine in its broken conjugate system.

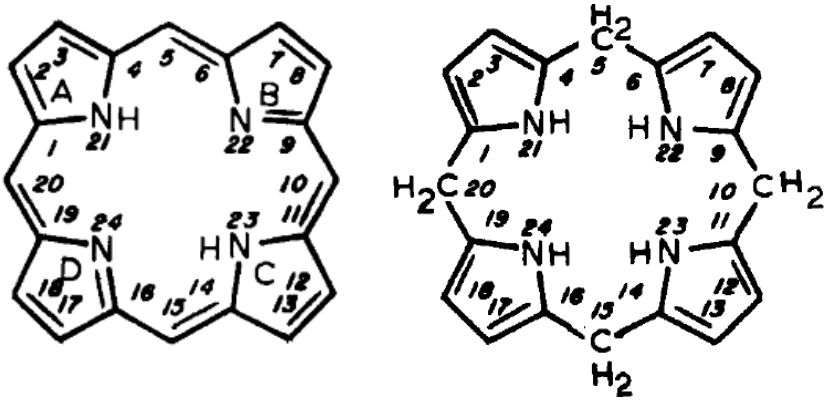

(a) porphine (b) porphyrinogen

Figure 1.6: Numbering tetrapyrrole carbon sites according to IUPAC. Pictures were taken from [5].

Important properties of porphyrin tetrapyrrole ring are:

1. ability to complex with anions.
2. absorbing in optical wavelenghts because of conjugation in macrocycle.

These two important properties can be tuned by appending another groups to porphyrin ring. In [6] we find study of properties of eight different porphyrins and porphyrinogens. One of them was meso-tetrakis(3,5-di-*tert*-butyl-4-hydroxyphenyl)porphyrin, shortly oxoporphyrin. Another studied molecules were porphyrinogen derivatives. One apparent difference between porphyrin and porphyrinogen was in UV-vis spectra. All porphyrinogens had one intense peak at around 505-518 nm whereas oxoporphyrin had intense band at 427 nm, see Figure 1.7. This illustrates essential change in conjugate system because of different tetrapyrrole substitution. Oxoporphyrin could reversibly interconvert to oxoporphyrinogen (OxP). Protonation of quinonoid oxygen simply transfers to two unsaturated pyrrolic nitrogen what is analogically accompanied with complete change in its conjugate system (Figure 1.8).

Optical spectrum and thus color of OxP is influenced by solvent polarity. This property is denoted solvatochromism. In [7] was studied sensibility of optical spectrum of OxP and its di-N-benzylated form to solvent polarity and complexation

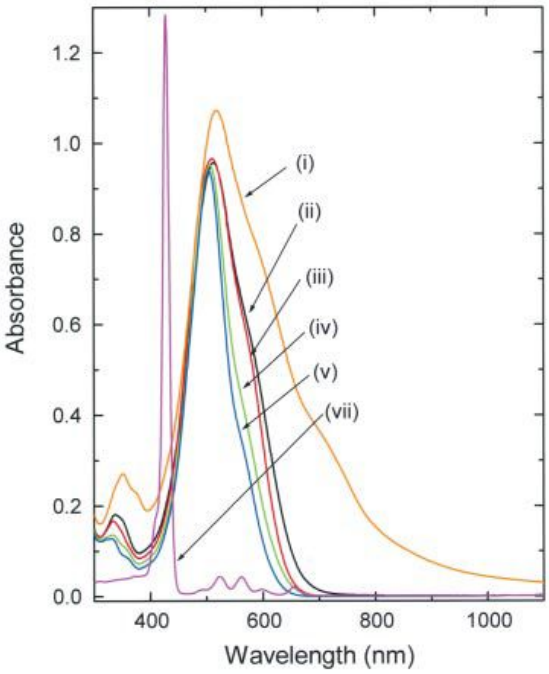

Figure 1.7: Optical absorption spectra of porphyrinogens (i)-(v) and oxoporphyrin (vii) in 1,2-dichlorbenzene. Adopted from [6].

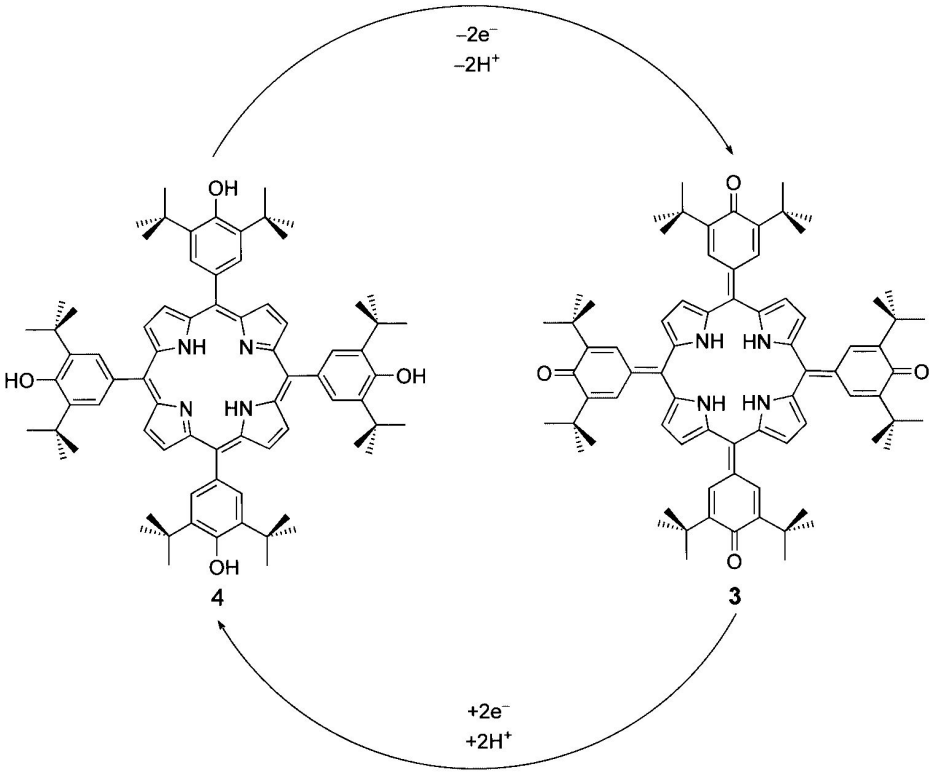

Figure 1.8: Reversible interconversion between oxoporphyrin (left) and oxoporphyrinogen (right). Adopted from [6].

with several anions. They revealed that both macrocycles create complexes with anions and can serve as colorimetric sensors of their presence.

Another paper [8] presents OxP and its derivatives as good sensor of trace

amount of water. This porphyrinogens create complexes with water and thus change their optical spectra. After making calibration curves, trace water up to around 50 ppm (related to number of solvent molecules) is detectable via optical spectrum (Figure 1.9).

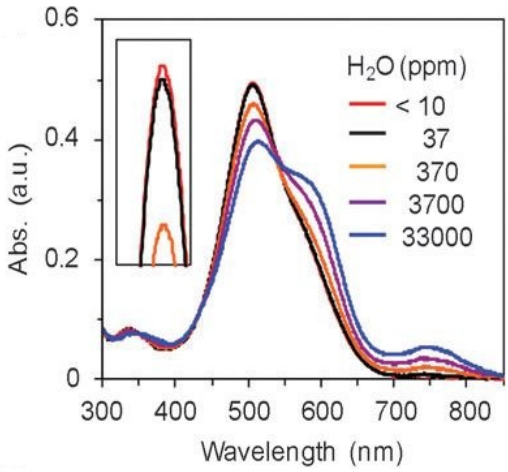

Figure 1.9: Optical spectrum of OxP with trace water in THF. Free porphyrinogen reveals band at 507 nm, water-complexed at 600 nm. Adopted from [8].

Recently a study about dynamic processes of OxP was published [9]. It describes qualitatively and quantitatively tautomerization (interconversion between two two-fold protonated forms of OxP) and inversion of tetrapyrrole macrocycle (ring-flip), see picture 1.10. In this study were used ^{1}H NMR spectroscopy and density functional theory calculations. Protonation and consequently also tautomerization of OxP was caused by presence of mandelic acid. The protonation even induced chirality[10] of OxP because both tautomers are mirror images to each other. Chiral mandelic acid then served as solvating agent (see below) and helped to distinguish the two OxP enantiomers. It was found that water influences both processes and can increase their rate constant a few times.

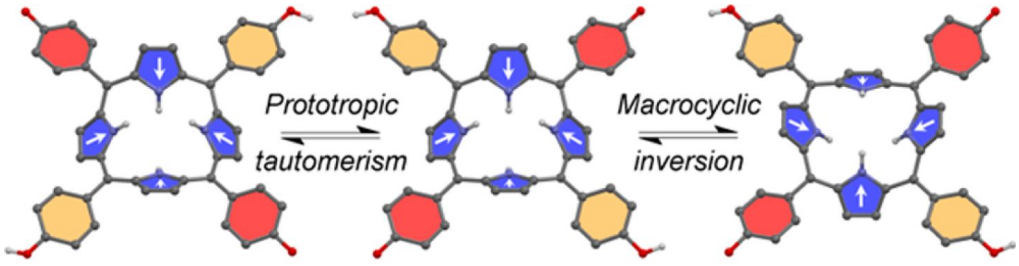

Figure 1.10: Dynamic processes in OxP. *Tert*-butyl groups are not depicted. Adopted from [9].

[10]As chiral are denoted molecules whose mirror images are not identical with the original molecule. Both mirror images are denoted as enantiomers and denoted as (R) and (S) forms (or (+) and (−) forms).

1.4.2 Porphyrins as sensors of chirality

Chirality is important property of certain molecules. This term is related with stereoisomers - molecules with the same functional groups but with their different space ordering. Two stereoisomers can be either enantiomers - if they are mirror images to each other or diastereomers in other case. The measure of enantiomeric purity is enantiomeric excess (ee) defined as:

$$ee = \frac{[R]_{tot} - [S]_{tot}}{[R]_{tot} + [S]_{tot}} \tag{1.36}$$

where $[R]_{tot}$ and $[S]_{tot}$ are total concentrations of (R)- and (S)-form of a chiral molecule, respectively. NMR could be used for determination of ee. Howewer, *NMR does not distinct between enantiomers*. Thus additional agent must be added into analyte. So far only chiral agents were used. There are three different approaches [10]:

1. chiral derivatizing agent - before measurement the analyte reacts with enantiopure agent while creating diastereomers with distinct NMR signals,

2. chiral solvating agents - during measurement the analyte creates diastereomeric complexes with enantiopure agent in regime of fast chemical exchange,

3. chiral lanthanide shift reagents - the same as above but chiral solvating agents contains lanthanoid atom (e.g. Eu, Pr) which increases chemical shift difference between both distinct diastereomeric forms of complex[11].

The phenomenon of determination ee by NMR using *achiral reagent* was first published in [11]. There host-guest complex of OxP and mandelic acid was investigated. Adding this chiral guest into pure host solution caused splitting of peaks due to *ortho*-cyclohexadien protons and pyrrolic β-protons. This splitting denoted $\Delta\delta$ is linear function of absolute value of guest ee because of fast chemical exchange of (R)- and (S)-form of guest in the host-guest complex (detailed discussion below). This measurement was accomplished at room temperature. UV-vis titration revealed binding ratio 1:2. It seems, OxP has two binding sites, both on NH groups in the middle of tetrapyrrole macrocycle. Adding mandelic acid also increased H^+ cation concentration and caused protonation of host carbonyl groups.

Next study [12] investigated chirality sensing with two other porphyrin derivatives tetraphenylporphine (TPP) and *meso*-tetrabutylporphine (TtBuP). As chiral guest were used 2-phenoxy propionic acid and ibuprofen. They revealed the same splitting of β-protons of TPP and TtBuP and even of *ortho*-phenyl protons of TPP linearly dependent on ee. However, in this case splitting was best observable at -32.5 °C.

All investigated porphyrin molecules have at least C_{2v} symmetry, it means symmetry with at least one mirror plane (Thus their mirror images are identical with the original molecules.). This symmetry causes that chemical shift of corresponding protons are the same. However, if achiral porphyrin creates complex

[11] Lanthanides are paramagnetic elements generating strong local magnetic field.

with chiral molecule the whole complex becomes chiral. It causes different chemical shifts and consequently splitting of corresponding porphyrin signals. This effect we call *chirality transfer*.

Next contribution to the topic of achiral *ee* sensing is paper [13]. Here the investigated porphyrin derivative was N_{21},N_{23}-bis(4-bromobenzyl)-5,10,15,20-tetrakis(3,5-di-*tert*-butyl-4- oxocyclohexadien-2,5-ylidene)porphyrinogen (shortly di-brombenzyled-oxoporphyrinogen, DiBrBzOxP), see Figure 1.11. They investigated complexation of DiBrBzOxP host with ten different chiral guest molecules. Through ^{1}H NMR titration in $CDCl_3$ complexation with guest molecules and chirality transfer from guest molecules to achiral host were confirmed. Observed complex stoichiometry was in all cases 1:1 because big brombenzyl groups hindered the second potential binding site at the another side of host. There are four protons on host sensitive to chirality transfer: β-protons at alkylated (■) and non-alkylated (■) pyrrole groups and both nonequivalent *ortho*-cyclohexadien protons (● and ●). It was again confirmed that splitting of this peaks due to chirality transfer linearly depends on guest *ee*.

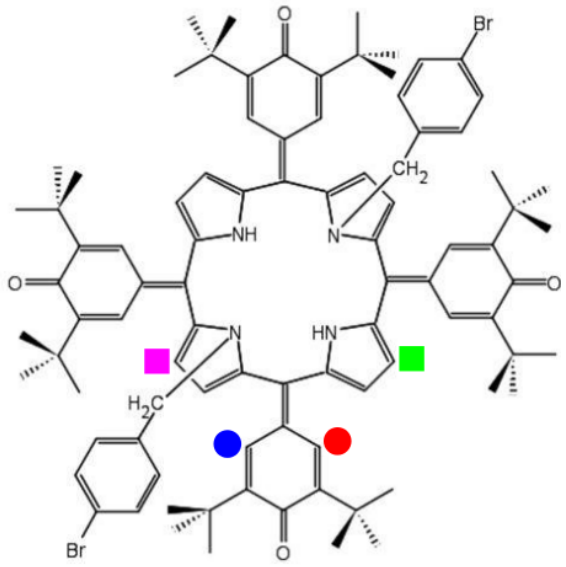

Figure 1.11: DiBrBzOxP

The latest contribution is work [14]. It contains overview of binding properties of three achiral porphyrin molecules TPP, OxP and DiBrBzOxP that are achiral sensors of chirality and comprises content of previous papers.

In conclusion of overview of works devoted to this topic we mention diploma thesis [15] in which complex of DiBrBzOxP with ibuprofen was investigated through ^{1}H NMR spectroscopy and theoretical density functional theory methods.

Now we elucidate mechanism of linear dependence of chirality transfer splitting $\Delta\delta$ on *ee*. Let us denote A, B protons that become nonequivalent after chirality transfer in host-guest complex. Chemical shifts[12] of proton A and B in complex with (*R*)- or (*S*)-form of chiral guest are denoted ${}^{R,S}\delta_A$ and ${}^{R,S}\delta_B$, respectively. Chemical shifts in free porphyrin are the same for both nuclei: ${}^{free}\delta_A = {}^{free}\delta_B$. Now we denote $f_{\mathbf{H},\,complex}$ and $f_{\mathbf{H},\,free}$ fractions of complexed and

[12]Note that chemical shifts ${}^{R,S}\delta_A$ and ${}^{R,S}\delta_B$ are *actual* chemical shifts of protons in host-guest complex while $\Delta\delta$ is value *observed* in NMR spectrum.

free host molecules. For observed chemical shifts of particular nuclei assuming fast exchange between (R)- and (S)-form of guest it holds:

$$\delta_{A\,obs} = f_{\mathbf{H},\,complex}({}^{R}\delta_A\; p_{\mathbf{HG}_R} + {}^{S}\delta_A\; p_{\mathbf{HG}_S}) + f_{\mathbf{H},\,free}\;{}^{free}\delta_A \tag{1.37}$$

and analogically

$$\delta_{B\,obs} = f_{\mathbf{H},\,complex}({}^{R}\delta_B\; p_{\mathbf{HG}_R} + {}^{S}\delta_B\; p_{\mathbf{HG}_S}) + f_{\mathbf{H},\,free}\;{}^{free}\delta_B\,, \tag{1.38}$$

where $p_{\mathbf{HG}_R}$ and $p_{\mathbf{HG}_S}$ are probabilities that chosen host-guest complex is formed by host and (R)-form of guest molecule or by its (S)-form, respectively[13]. After subtracting 1.38 from 1.37 we obtain

$$\Delta\delta \equiv \delta_{A\,obs} - \delta_{B\,obs} = f_{\mathbf{H},\,complex}({}^{R}\delta_A\; p_{\mathbf{HG}_R} + {}^{S}\delta_A\; p_{\mathbf{HG}_S} - {}^{R}\delta_B\; p_{\mathbf{HG}_R} - {}^{S}\delta_B\; p_{\mathbf{HG}_S})\,. \tag{1.39}$$

Now we assume that

$$p_{\mathbf{HG}_R} = \frac{[\mathbf{G}_R]_{tot}}{[\mathbf{G}_R]_{tot} + [\mathbf{G}_S]_{tot}} \tag{1.40}$$

$$p_{\mathbf{HG}_S} = \frac{[\mathbf{G}_S]_{tot}}{[\mathbf{G}_R]_{tot} + [\mathbf{G}_S]_{tot}}\,, \tag{1.41}$$

$[\mathbf{G}_R]_{tot}$ and $[\mathbf{G}_S]_{tot}$ are total concentrations of particular enantiomers of guest. Because of mirror symmetry of (R)- and (S)-form of guest and C_{2v} symmetry of host it holds:

$${}^{R}\delta_A = {}^{S}\delta_B \tag{1.42}$$

$${}^{S}\delta_A = {}^{R}\delta_B\,. \tag{1.43}$$

Then

$$f_{\mathbf{H},\,complex}({}^{R}\delta_A - {}^{R}\delta_B) = -f_{\mathbf{H},\,complex}({}^{S}\delta_A - {}^{S}\delta_B) \equiv \Delta\delta_{max} \tag{1.44}$$

and the resulting equation is:

$$\Delta\delta = \Delta\delta_{max}\, ee\,, \tag{1.45}$$

where $\Delta\delta_{max}$ is maximal splitting in presence of pure enantiomer ($ee = 1$ or $ee = -1$). However, in the NMR spectrum we can only resolve the absolute value of $\Delta\delta$. Therefore only adding certain amount of pure enantiomer into sample enables determining of ee sign.

[13] It holds $p_{\mathbf{HG}_R} + p_{\mathbf{HG}_S} = 1$.

1.5 Goals of this work

As described above sensing of *ee* via complexation of chiral analyte with DiBr-BzOxP (see above in the Figure 1.11) was proved for several molecules. Goal of this work is to confirm possibility of chirality sensing for another chiral molecule *camphorsulfonic acid* (Figure 1.12) via NMR. We have to find out whether this

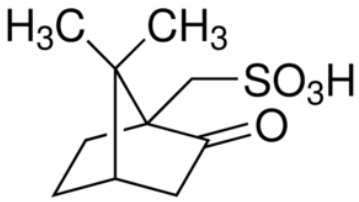

Figure 1.12: (*R*)-camphorsulfonic acid.

two chemicals form complex. Important is to determine stoichiometry of the complex and find association constant $K_{\mathbf{HG}}$. Next step is to detect which nuclei are sensitive to *ee* and then to prove linear dependence of their chemical shift on *ee*.

Camphorsulfonic acid is a strong acid so we have to determine whether DiBr-BzOxP becomes protonated and how it influences formation of the complex.

Quantum mechanical computations should reveal possible conformations of the complex and we will calculate its NMR spectra which could be compared to experiment.

Chapter 2

Results

2.1 NMR spectroscopy

2.1.1 Samples and experimental equipment

Porphyrin DiBrBzOxP (host, **H**) and (*R*)-,(*S*)-camphorsulfonic acid (guest, $\mathbf{G}_R$, $\mathbf{G}_S$) in crystallic form were obtained from National Institute for Materials Science, Tsukuba, Japan. In all experiments deuterated chloroform (Sigma Aldrich) stabilized by silver foil with internal standard tetramethylsilan (TMS) was used. All chemical shifts are referenced to TMS. NMR experiments were performed on Bruker Avance 500 spectrometer operating at 500.1 MHz. Typical measurement conditions were as follows: relaxation delay 2 s, spectral width 10 kHz, aquisition time 3.28 s, 16 - 48 scans. 1D spectra were aquisited after application of $\pi/2$ pulse (pulse width 8.5 μs). Bruker `cosy45` pulse sequence with resolution 2048 data points in the F2 dimension and 512 data points in the F1 dimension was used.

The temperature was maintained constant within ± 0.2 °C using BVT 3000 temperature unit. Low temperatures were achieved by nitrogen cooling.

2.1.2 Spectra of pure substances

Host

1D spectrum of DiBrBzOxP (0.6 mmol/l) as obtained at room temperature (25 °C) can be seen in the Figure 2.1[1]. Peaks were assigned according to ^{1}H COSY and NOESY experiments ([13]). From Figure 2.1 it is apparent that porphyrin sample contains certain amount of water. According to [13] and [8] host DiBrBzOxP forms complex with water and this significantly influences chemical shift of NH peak.

Guest

Spectrum of camphorsulfonic acid (17.9 mmol/l) can be seen in Figure 2.2. Well distinguished peaks were assigned according to the internet database http://sdbs.db.aist.go.jp

[1] Only one of all protons with equivalent chemical shift is denoted, chemical shifts of methyl protons are averaged due to fast rotation of the whole methyl group.

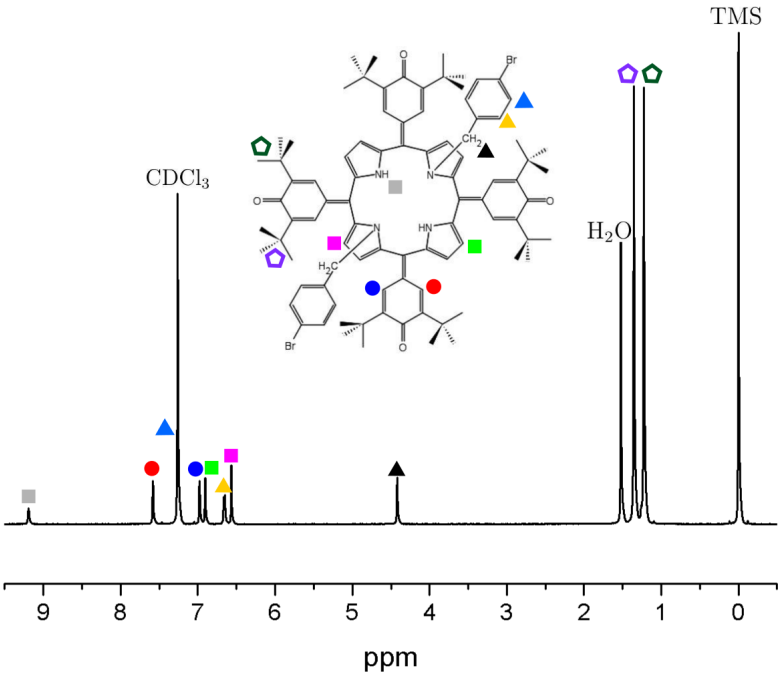

Figure 2.1: ^{1}H NMR spectrum of pure DiBrBzOxP in $CDCl_3$ at room temperature.

and ^{1}H COSY and NOESY experiments. The OH peak is broadened because of fast chemical exchange with water.

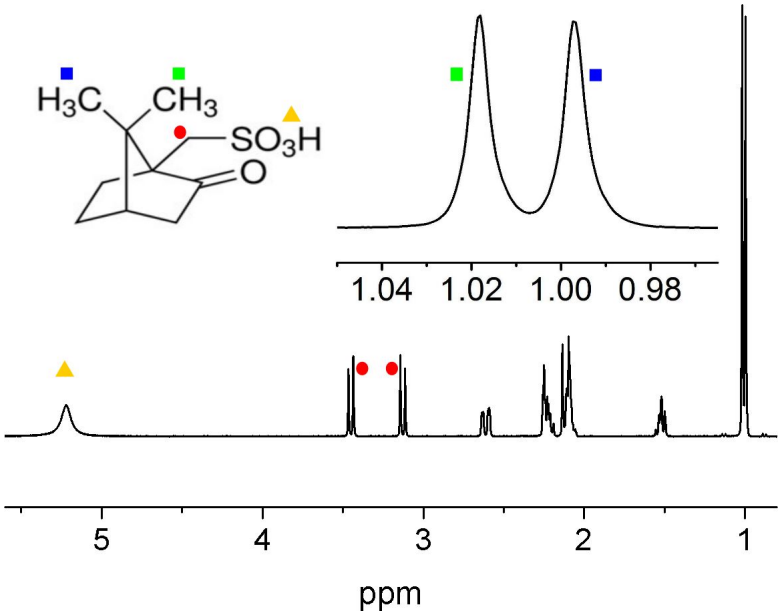

Figure 2.2: ^{1}H NMR spectrum of pure (*R*)-camphorsulfonic acid in $CDCl_3$ at room temperature.

2.1.3 Titration experiments

The NMR titration consists of acquisition of many spectra with different ratio of host/guest concentrations. It allows determination of association constant and

reveals details about complexation. We made two different titration experiments - with pure (R)-form of guest and then with its racemic mixture, both titrations were performed at room temperature. In the samples there was constant amount of host and guest was added up to over 50 eq. Much higher concentration of guest was limited by its solubility. Host concentration in the samples was about[2] 0.6 mmol/l. Molar ratios (equivalents, eq[3]) of guest and host were determined from NMR spectra by comparing areas of non-overlapping peaks of guest methyl groups (1.02 and 0.96 ppm in pure guest spectrum, Figure 2.2) and host *tert*-butyl groups (1.35 and 1.23 ppm in pure host spectrum, Figure 2.1).

Important changes in spectra due to complexation

At first we focus on NH peaks (Figure 2.3). Both titrations with (R)- and racemic

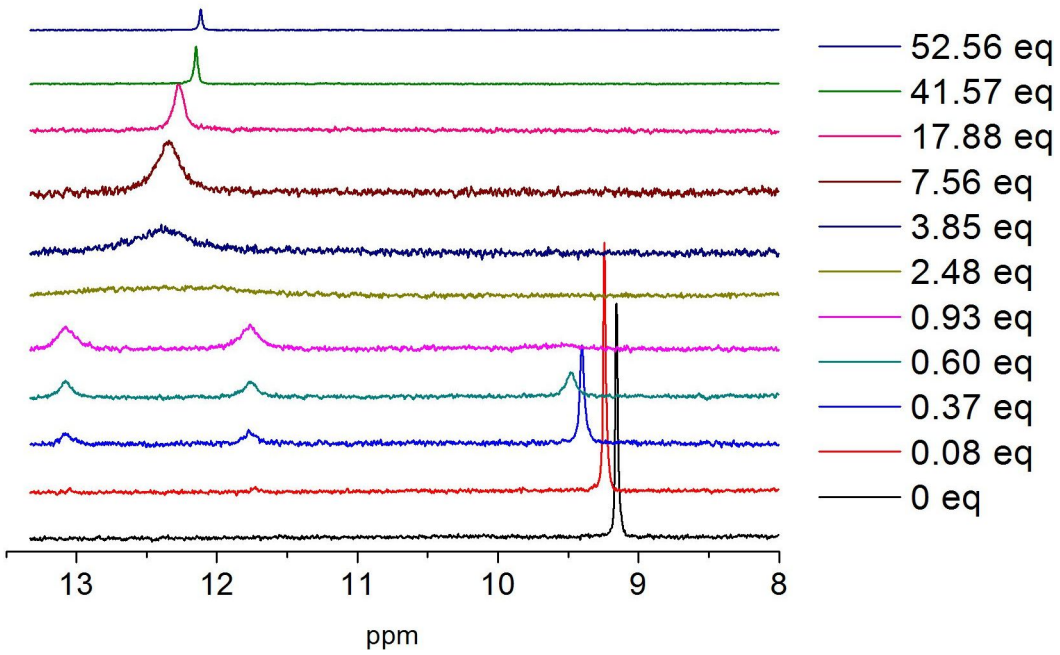

Figure 2.3: Partial ^{1}H NMR spectra (NH peaks) as obtained during titration of DiBrBzOxP with (R)-camphorsulfonic acid performed in $CDCl_3$ at room temperature.

form of guest revealed the same behavior. Up to 1 eq we can distinguish three NH peaks: free host at 9.16 ppm slightly moving downfield[4] with increasing guest concentration and two peaks at 11.73 and 13.05 ppm which belong to NH groups in host-guest complex. Both NH peaks of complexed host have the same area and their intensity corresponds to signal from one proton. So we conclude that they originate from the same complexed molecule[5]. In the spectrum measured for 1

[2]Actually, the concentration of host decreased moderately to 0.4 mmol/l during titration because of dilution by stock solution of guest.

[3]As equivalent (eq) we denote relative number of water or guest molecules compared with number of host molecules.

[4]Term downfield refers to high ppm values and vice versa.

[5]Exactly from a few different conformations which corresponding chemical shifts are averaged.

equivalent of guest, NH peak of free porphyrin vanishes. It suggests complexation in the ratio 1:1. It will be proven more precisely in the text below. Above 1 eq both NH peaks of complexed porphyrin coalesce due to faster exchange of bound guest at higher concentrations.

Now we analyse peak of β-protons that are bound to alkylated pyrrole in macrocycle (Figure 2.4, ■ at 0 eq). In case of free porphyrin it appears at 6.57 ppm. But in the complex both pairs of this β-protons become nonequivalent (chirality transfer) and emerge typical doublet of doublets at around 6.90 ppm (Figure 2.4, ■ at 2.82 eq). This AB system is of particular importance because it is sensitive to guest *ee* (details in the next chapter). Assignment of peaks was supported by ^{1}H COSY spectrum (Figure 2.6): AB system (■) that appears at 6.90 ppm for 5.09 equivalents of guest reveals J-coupling only between itself but not with other peaks in the spectrum so we suggest it is β-proton that was originally at 6.57 ppm in spectrum of pure host (Figure 2.4, ■ at 0 eq). This suggestion is supported by QM computations of chemical shifts (Table 2.5). In the case of titration with racemic mixture of guest this doublet of doublets shrinks to one singlet because of chemical exchange between $\mathbf{G}_R$ and $\mathbf{G}_S$ (Figure 2.5, ■ at 2.82 eq). Assignment of other peaks as seen in the Figures 2.4 and 2.5 is based on COSY spectrum (Figure 2.6) and by comparing with assigned spectrum of pure host.

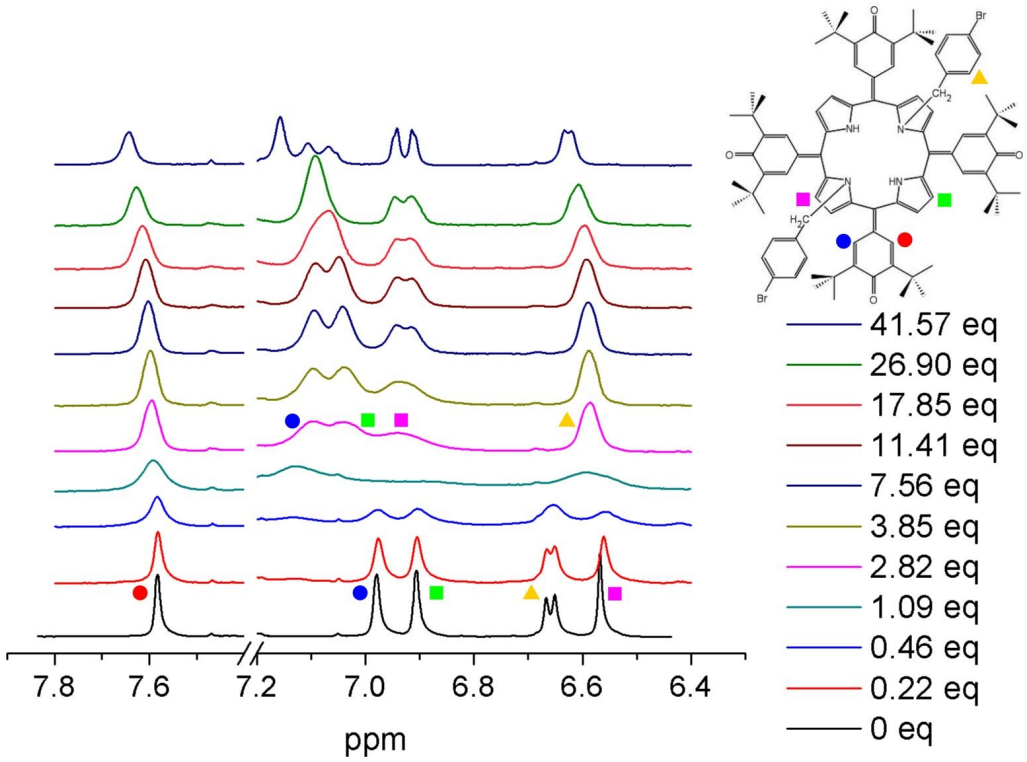

Figure 2.4: Partial ^{1}H NMR spectra as obtained during titration of DiBrBzOxP with (*R*)-camphorsulfonic acid performed in $CDCl_3$ at room temperature.

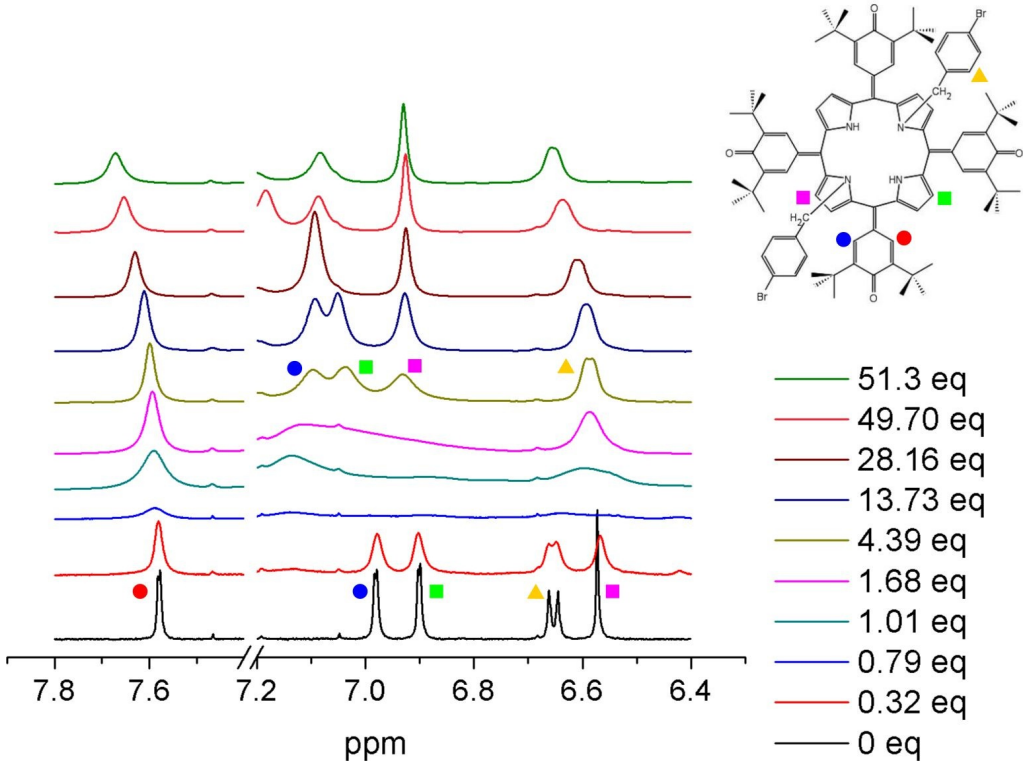

Figure 2.5: Partial ^{1}H NMR spectra as obtained during titration of DiBrBzOxP with racemic camphorsulfonic acid performed in $CDCl_3$ at room temperature.

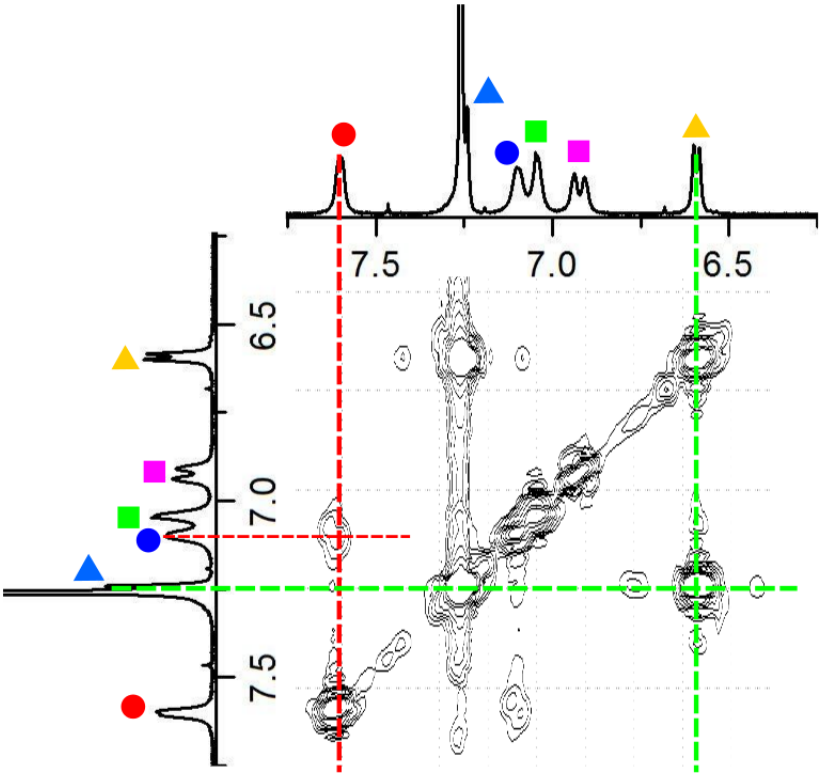

Figure 2.6: ^{1}H COSY spectrum of DiBrBzOxP in the presence of 5.09 eq of (*R*)-camphorsulfonic acid in $CDCl_3$ at room temperature. Colored symbols denoting particular resonances correspond to that in the Figure 2.1

.

Determination of complex stoichiometry and association constant

Our first goal is determination of association constant of complex $K_{\mathbf{HG}}$ (equation 1.24). We can obtain its value from changes of NMR spectra during titration by a few ways.

First way consists in fitting dependence of fraction of complexed host

$$f_{\mathbf{H},\,complex} = \frac{[\mathbf{HG}]}{[\mathbf{H}]_{tot}} \tag{2.1}$$

on guest concentration with appropriate equation for binding isotherm. This values could be obtained from areas of NH peaks which correspond to free and complexed porphyrin. Using the definition 2.1 and equation 1.27 we obtain the appropriate binding isotherm in the form:

$$f_{\mathbf{H},\,complex} = \frac{K_{\mathbf{HG}}([\mathbf{H}]_{tot} + [\mathbf{G}]_{tot}) + 1 - \sqrt{[K_{\mathbf{HG}}([\mathbf{H}]_{tot} - [\mathbf{G}]_{tot}) - 1]^2 + 4K_{\mathbf{HG}}[\mathbf{H}]_{tot}}}{2K_{\mathbf{HG}}[\mathbf{H}]_{tot}}. \tag{2.2}$$

The shape of NH peak of free host and the two NH peaks of complexed host were fitted using simple Lorentzian line shape (equation 1.9) and symmetrical two-state chemical exchange shape (equation 1.11), respectively. In fact this phenomenon should be described exactly by asymmetrical three-state chemical exchange model. However, for low guest concentrations (below 1 eq) chemical exchange is slow

and all three peaks practically have a shape of broadened Lorentzian curve that could be well fitted with the mentioned model. At higher guest concentrations (above 1 eq) amount of free host is negligible so two state model is appropriate. Then obtained peak areas were recalculated to fraction (equation 2.1) and fitted by binding isotherm 1.27. Fitting of chemical exchange requires three constant parameters: chemical shifts of pure states without exchange (δ_{A0}, δ_{B0}; A and B denote states in chemical exchange) and width of both peaks without exchange (R_A, R_B, assuming $R_A = R_B$). These parameters were obtained by fitting spectrum with the smallest amount of guest by assuming rate constant $k = 0$. The middle of both NH peaks of complexed porphyrin moves with increasing guest concentration so we set difference of their chemical shifts fixed but absolute value of these shifts as fitted parameter. Another fitted parameters were rate constant k and linear scaling parameter M. All fitting procedures in this work were carried out by solver tool in the programme *Excel* 2003.

In Figure 2.7 experimental points and fitted binding isotherm (magenta solid line) as obtained from titration of $\mathbf{G}_R$ into a solution of **H** are shown. We can see a sharp 'knee' at concentration 1 eq and above 1 eq all values of $f_{\mathbf{H},\,complex}$ equal 1 as peak of free porphyrin vanished (see Figure 2.3). It clearly indicates 1:1 stoichiometry binding model. After fitting the value $K_{\mathbf{HG}} = 8 \times 10^{13}$ l/mol was obtained.

Unfortunately this value is not real since values $f_{\mathbf{H},\,complex}$ around 1 eq have great influence on $K_{\mathbf{HG}}$ and a small experimental error cause wide variations in $K_{\mathbf{HG}}$. In the Figure 2.7 our guess of error around 1 eq is shown. Around 1 eq the peak due to free porphyrin is too wide and is practically lost in noise (see the Figure 2.3). Thus here the experimental error is relatively large. Even binding isotherm with $K_{\mathbf{HG}}$ which differs by several orders (green dashed line in the Figure 2.7, this value will be determined in the next part of this section) from the fitted value is in frame of this experimental error. Titration of racemic **G** into a solution of **H** gave qualitatively the same dependence of $f_{\mathbf{H},\,complex}$ on guest concentration and fitting with theoretical binding isotherm gave also unrealistic value $K_{\mathbf{HG}} = 5 \times 10^{20}$ l/mol.

Now let us look at another change in spectra during titration which consists in change of chemical shift of guest methyl groups. The chemical shift is increasing with guest concentration (see Figure 2.8). Another way to determine association constant is processing the observed difference of chemical shift of these guest methyl signals denoted as $\delta_{1\,obs}$ and $\delta_{2\,obs}$ ($\delta_{1\,obs} > \delta_{2\,obs}$). Their difference $\Delta\delta_{obs} \equiv \delta_{1\,obs} - \delta_{2\,obs}$ as function of guest concentration is depicted in the Figure 2.9.

Note that for low guest concentration chemical exchange of two NH peaks due to complexed host was *slow* (see Figure 2.3, 11.5 - 13 ppm). But in the case of guest methyl resonances the exchange is always *fast* because instead of four peaks that would correspond to free and complexed guest we see only two averaged peaks in the spectrum for arbitrary guest concentration. This ostensible discrepancy has the following explanation: guest molecules in host-guest complexes are under fast exchange but host NH peaks are sensitive not only to this fast guest exchange but also to protonation of host carbonyl group which undergoes slow exchange. Detailed discussion on effects of protonation would be introduced in the last section of this chapter.

So now we assume fast exchange instead of slow exchange as assumed for NH

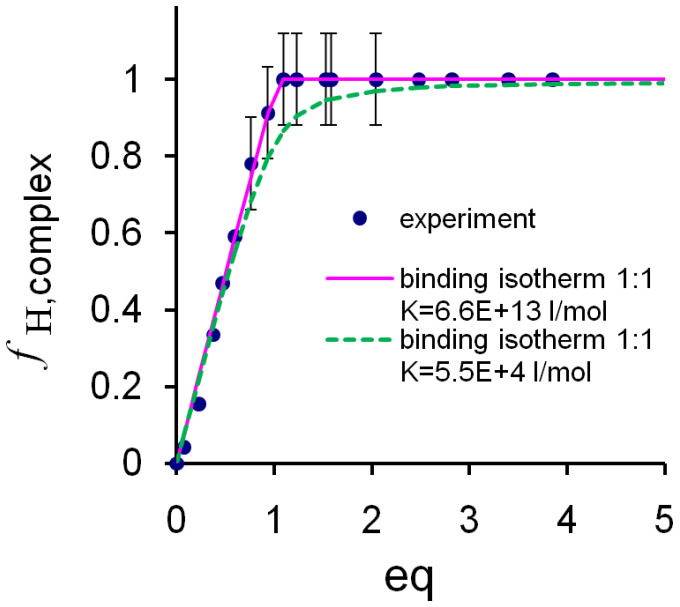

Figure 2.7: Experimental values of complexed host fraction $f_{\mathbf{H},complex}$ obtained from titration of DiBrBzOxP with (R)-camphorsulfonic acid. Data fitted with 1:1 binding isotherm (according to equation 2.2, solid magenta line). Guess errorbars are shown around 1 eq. Binding isotherm with another value of $K_{\mathbf{HG}}$ as will be obtained in the next section is depicted (green dashed line).

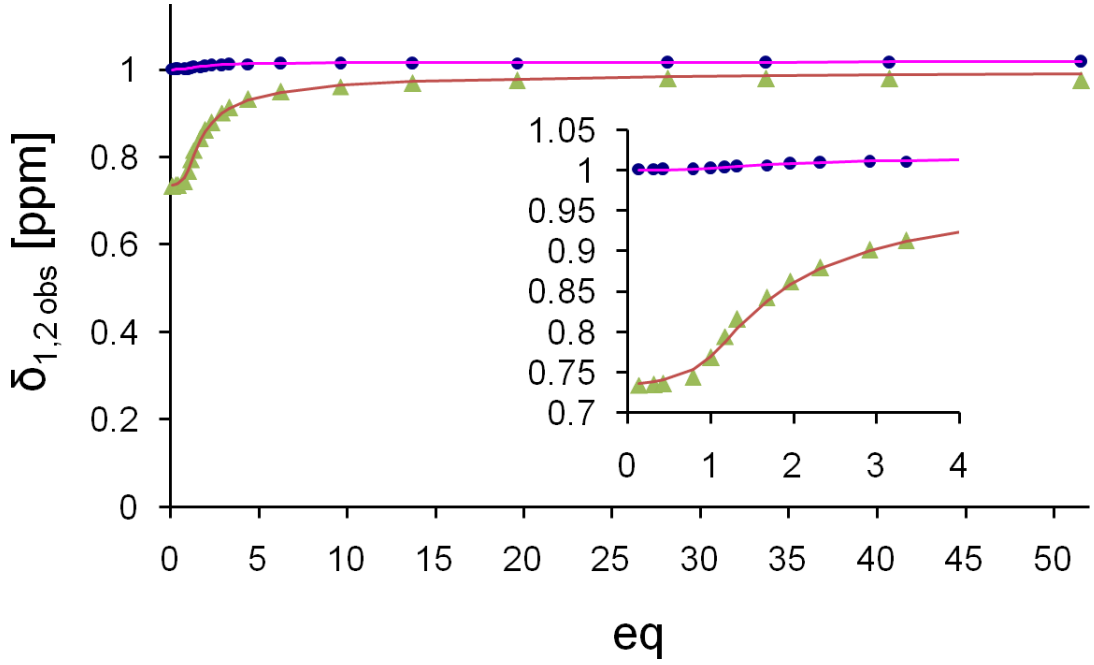

Figure 2.8: Observed guest methyl peak shifts during titration of DiBrBzOxP with racemic camphorsulfonic acid, fitted with 1:1 binding isotherm (according to equation 2.6).

peaks. Fitting procedure again expects 1:1 stoichiometry.

Let us denote

$$f_{\mathbf{G},\,free} \equiv \frac{[\mathbf{G}]}{[\mathbf{G}]_{tot}} \tag{2.3}$$

and

$$f_{\mathbf{G},\,complex} \equiv \frac{[\mathbf{HG}]}{[\mathbf{G}]_{tot}} \tag{2.4}$$

as fractions of free and complexed guest molecules. Of course, it holds:

$$f_{\mathbf{G},\,free} = 1 - f_{\mathbf{G},\,complex}\,. \tag{2.5}$$

Then using the above definitions and equation 1.27 we obtain:

$$f_{\mathbf{G},\,complex} = \frac{K_{\mathbf{HG}}([\mathbf{H}]_{tot} + [\mathbf{G}]_{tot}) + 1 - \sqrt{[K_{\mathbf{HG}}([\mathbf{H}]_{tot} - [\mathbf{G}]_{tot}) - 1]^2 + 4K_{\mathbf{HG}}[\mathbf{H}]_{tot}}}{2K_{\mathbf{HG}}[\mathbf{G}]_{tot}}\,. \tag{2.6}$$

Now we label the actual shift differences of free and complexed guest $\Delta\delta_{free}$, $\Delta\delta_{complex}$, respectively. Considering fast exchange the appropriate binding isotherm reads:

$$\Delta\delta_{obs} = \Delta\delta_{free}\, f_{\mathbf{G},\,free} + \Delta\delta_{complex}\, f_{\mathbf{G},\,complex}. \tag{2.7}$$

As parameter $\Delta\delta_{free}$ we take value 0.21 ppm which was obtained from pure guest spectrum (In the limit of high guest concentration the amount of complexed guest would be negligible and we would see only shifts of free guest.). Fitted parameters were $\Delta\delta_{complex}$ and $K_{\mathbf{HG}}$.

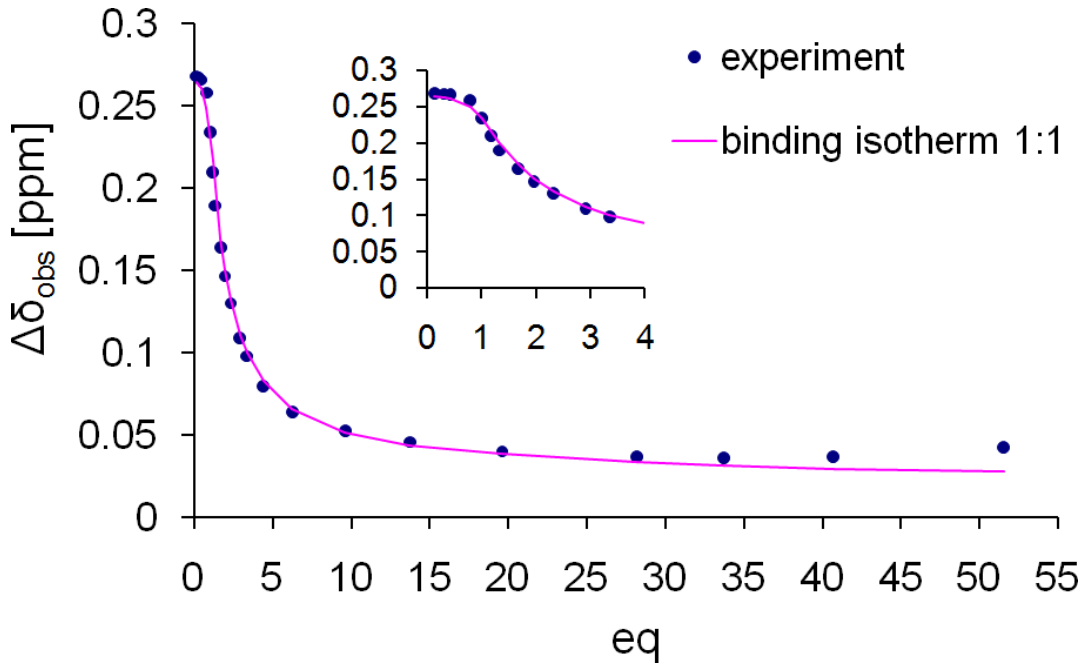

Figure 2.9: Observed difference in methyl peaks' shifts during titration of DiBrBzOxP with racemic camphorsulfonic acid. Experimental values were fitted with corresponding 1:1 binding isotherm 2.6.

Equilibrium association constant values obtained from this fitting are 5.5×10^4 l/mol from titration of $\mathbf{G}_R$ into $\mathbf{H}$ and 4.7×10^4 l/mol from titration of racemic $\mathbf{G}$ into $\mathbf{H}$. These values are much more realistic.

Determination of association constant from UV-Vis titration

Absorption UV-vis spectrum is sensitive to protonation of porphyrin. However, this protonation strongly coincidences with formation of host-guest complex because host protonation creates energetically favourable binding site for negatively charged guest molecules. Therefore, equilibrium constant of host protonation is very similar to equilibrium association constant of host-guest complex and UV-vis titration can be used for determination of the association constant.

We received data from UV-vis titration of DiBrBzOxP with (*S*)-camphorsulfonic acid measured in NIMS, Japan. Data were measured on spectrophotometer JASCO J-810. Analogically to NMR titration, amount of porphyrin was constant[6] and guest was added from stock solution up to concentration 5 eq. According to the Figure 2.10 three absorption peaks were observed: at 500 nm with shoulder at 560 nm and at 753 nm. As signed in the graph with red arrows, with growing number of guest equivalents intensity of the absorption peak at 500 nm is decreasing while intensity of its shoulder at 560 nm is increasing and intensity of the smaller peak at 753 nm is increasing. The straightforward conclusion is that the most intensive peak at 500 nm belongs to free porphyrin while the other two peaks belong to porphyrin complex with guest. To determine association constant $K_{\mathbf{HG}}$ absorbance at absorption maximum 753 nm was fitted (Figure 2.11). The fitting binding isotherm 1:1 was derived on the assumption that absorbance A is direct proportional to complexed host concentration [**HG**]:

$$A_{\mathbf{H},\,complex} = \epsilon l[\mathbf{HG}], \tag{2.8}$$

where ϵ is extinction coefficient and l is sample thickness. Taking this expression together with the equation 1.27 we obtain corresponding binding isotherm:

$$A_{\mathbf{H},\,complex} = \epsilon l \frac{K([\mathbf{H}]_{tot} + [\mathbf{G}]_{tot}) + 1 - \sqrt{[K([\mathbf{H}]_{tot} - [\mathbf{G}]_{tot}) - 1]^2 + 4K[\mathbf{H}]_{tot}}}{2K}. \tag{2.9}$$

As mentioned in footnote host solution gets more diluted with adding guest so after saturation over 1 eq absorbance of 753 nm peak decreases moderately instead of being constant. However, during the fitting procedure dilution was accounted and fit revealed value $K_{\mathbf{HG}} = 1.07 \times 10^5$ l/mol. This value differs by factor of two from those obtained by NMR titration values.

[6] In fact, porphyrin concentration was reduced by diluting with adding guest from stock solution. This has effect of spectra - see below in text.

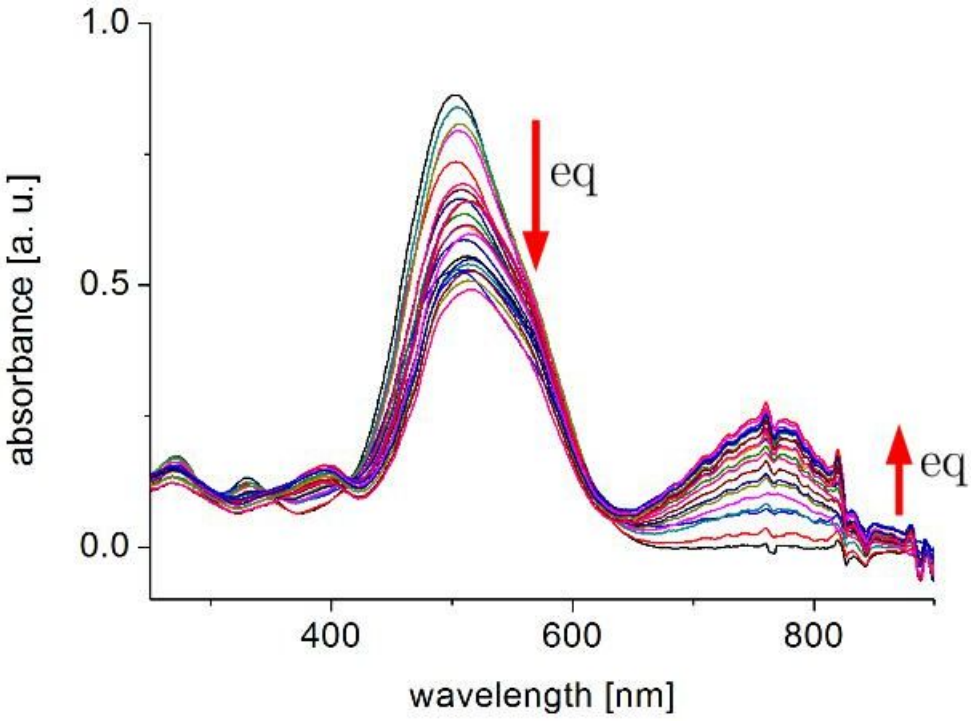

Figure 2.10: UV-Vis titration of DiBrBzOxP with (*S*)-camphorsulfonic acid in concentration range 0-5 eq performed in $CDCl_3$ at the room temperature.

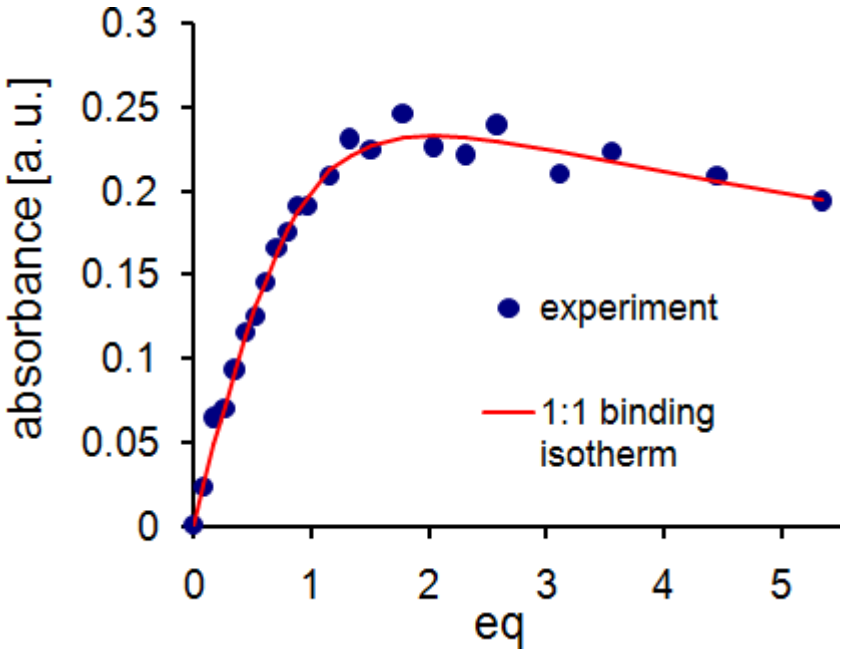

Figure 2.11: Fitting absorbance change at 753 nm with 1:1 binding isotherm.

Formation of host-guest complex with higher stoichiometry

As can be seen in the Figures 2.4 and 2.5, all peaks are effected by chemical exchange, therefore, their chemical shift and their width is changed with increasing guest concentration. Chemical exchange influences also shifts of the both host *tert*-butyl peaks. We plotted dependence of their chemical shift $\delta_{1\,obs}$ and $\delta_{2\,obs}$ on guest concentration, see Figure 2.12. Both titrations of host with (*R*)-

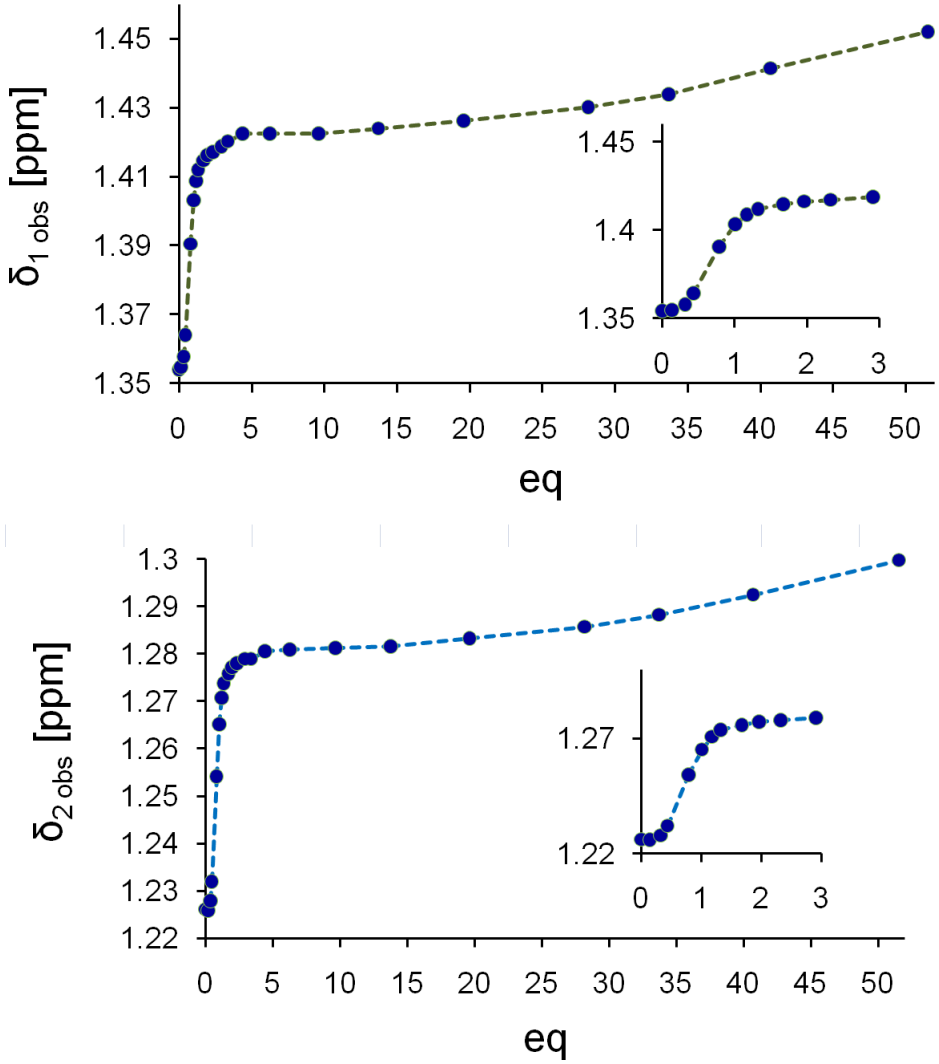

Figure 2.12: Observed chemical shift of both *tert*-butyl resonances of DiBrBzOxP as function of racemic camphorsulfonic acid concentration. Experimental points are connected by dashed lines (not fitted).

form of guest and with its racemic mixture reveal the same behavior. The 'knee' at around 1 eq reflects already described formation of 1:1 host guest complex. However, if only this effect was present, shift of the peaks above 1 eq would be constant. Therefore another effect must be present. As would be seen below in the chapter devoted to quantum chemical computations, calculated electrostatic potential surfaces indicates four potential binding sites for positively charged parts of molecules at the four carbonyl groups (Figure 2.19a). This effect cannot be protonation of more than one host carbonyl groups because such effect would be seen in the UV-vis spectra. Thus we suggest forming of host-guest complex

with higher stoichiometry than 1:1. Probably guest molecules are bound through SO_3H group to host carbonyles through hydrogen bond.

2.1.4 Sensitivity to guest chirality, determination of enantiomeric excess

As mentioned in previous chapter induced chemical shift non-equivalency (splitting) of β-proton peaks (at 6.9 ppm) linearly depends on enantiomeric excess (*ee*). This phenomenon could be used for determination of *ee* if $\Delta\delta_{max}$ (dependent on number of eq) is known (equation 1.45). However, this splitting can be fitted and consequently quantitatively processed only at higher guest concentrations because at lower concentrations intermediate chemical exchange beween non-complexed and complexed states broadens the peaks, see Figure 2.4. To investigate guest chirality effects on host spectrum another measurements of NMR spectra at 28 eq[7] of guest with various *ee* of guest were performed. Our measurements are depicted in the Figure 2.13. Exact value of *ee* in samples was achieved by weighting and mixing exact amount of pure forms of camphorsulfonic acid enantiomers in crystallic form.

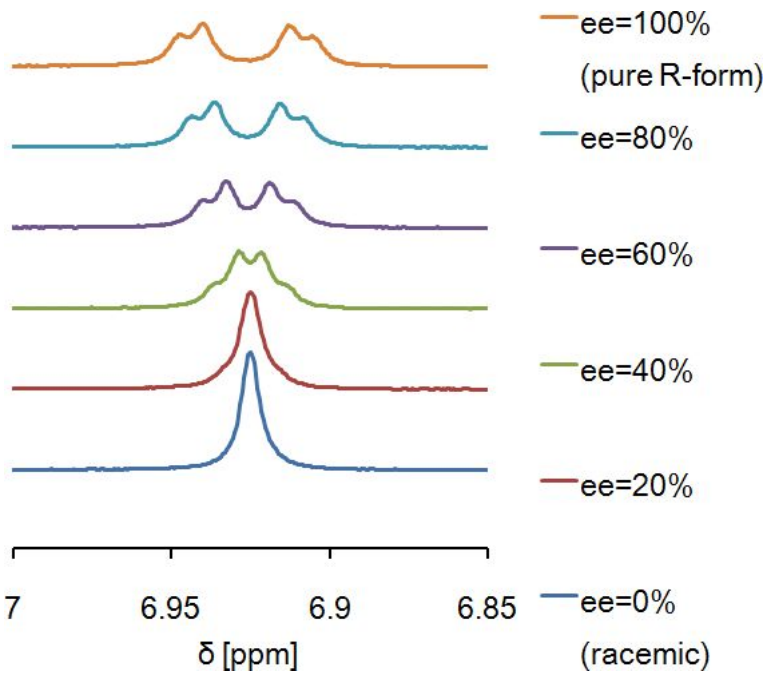

Figure 2.13: Peaks of β-protons in host-guest complex depending on guest enantiomeric excess. Spectra were recorded with guest concentration around 28 eq.

As we wrote in the first chapter the observed splitting due to chirality $\Delta\delta$ could be described by fast exchange with this form:

$$\Delta\delta = \Delta\delta_{max}\, ee\,.$$

[7]Spectrum measured by titration **H** with $\mathbf{G}_R$ at 26.90 eq (Figure 2.4) shows too broad peaks unlike this measurements. But it is probably only effect of bad shimming because temperature was the same.

Fitting with corresponding peak shapes of AB system (equations 1.13, 1.14 and 1.15) confirmed this linear dependence as can be seen in the Figure 2.14 and revealed the value $\Delta\delta_{max} = 0.034$ ppm.

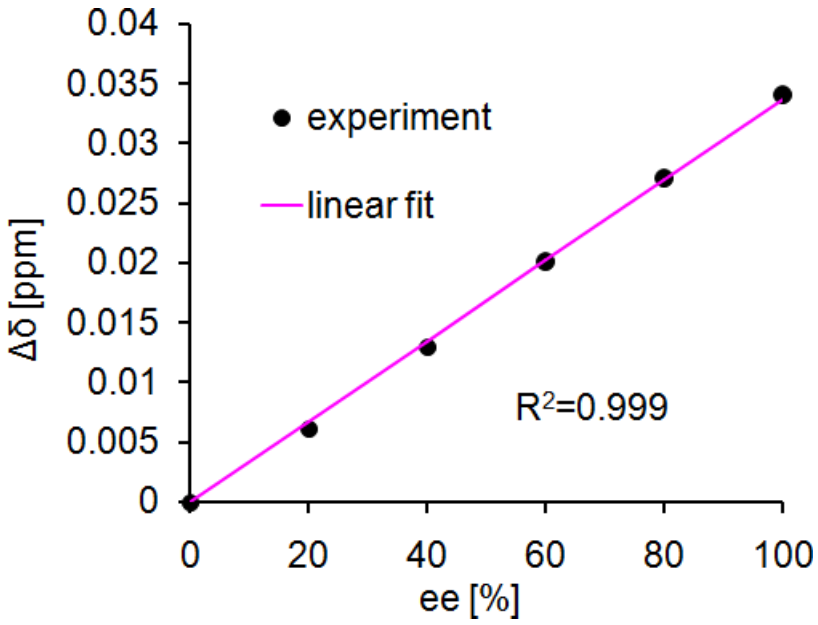

Figure 2.14: Fitting of linear dependence of observed difference in β-proton chemical shifts on guest enantiomeric excess. Spectra were measured at 28 eq of guest.

2.1.5 Variable temperature measurement

Host-guest complexation is not the only process taking place in our samples. With respect to ^{1}H spectrum of pure camphorsulfonic acid (Figure 2.2) we know that deprotonation of its OH group is a frequent event. We already know from papers mentioned in the first chapter ([6], [9]) that four carbonyl groups of porphyrin molecule can be subject to protonation. Their protonation can induce change in chemical shift of *tert*-butyl or *ortho*-cyclohexadienylidene protons because of their mutual vicinity.

We will investigate host protonation at low temperature when all chemical processes go slower and NMR peaks represent particular states instead of their averages.

We performed measurements of ^{1}H NMR spectra at low temperatures for four samples with variable guest concentration and enantiomeric excess:

1. **H** in presence of 0.6 eq $\mathbf{G}_R$,
2. **H** in presence of 0.5 eq of racemic **G**,
3. **H** in presence of 13.7 eq $\mathbf{G}_R$,
4. **H** in presence of 16.7 eq of racemic **G**.

Equivalents were determined by fitting both host *tert*-butyl and both guest methyl peaks at room temperature measurement. However, under 1 eq peaks were slightly deformed and resulting numbers are not too accurate. In addition, solubility of guest changes with temperature and it influences the number of dissolved guest molecules. Thus number of eq can change with temperature. We performed two series of measurements for guest concentrations lower then 1 eq to observe peaks due to both protonated and non-protonated host and two series of measurements for concentrations higher then 1 eq to see effects only with protonated porphyrin. The measurements were taken in temperature region from -55 °C to 60 °C. Lower temperatures were not possible because of sample freezing.

Variable temperature effects on guest methyl peaks

Let us focus on the upfield spectral region with signals from host *tert*-butyl and guest methyl groups depicted in the Figures 2.15a, 2.15b, 2.16a and 2.16b. Guest methyl signals for both series of measurements (with (R)- and racemic form) below 1 eq change their chemical shift only slightly. Binding isotherm reveals that practically all guest molecules are in the complexed state (The association constant $K_{\mathbf{HG}}$ is relatively high.). Signal at 0.95 ppm (■) splits into two inequal peaks at low temperature, it means that guest molecules are located in two different conformations of complex, we denote them HG1 and HG2. Areas of these two peaks (magenta and blue arrow in the Figures 2.15a and 2.16a) reveal relative population[8] of this complex (HG1):(HG2) 0.35:0.65.

[8] All peaks in spectra obtained by low temperature measurement were fitted with the Lorentzian curves .

(a) 0.59 eq of guest

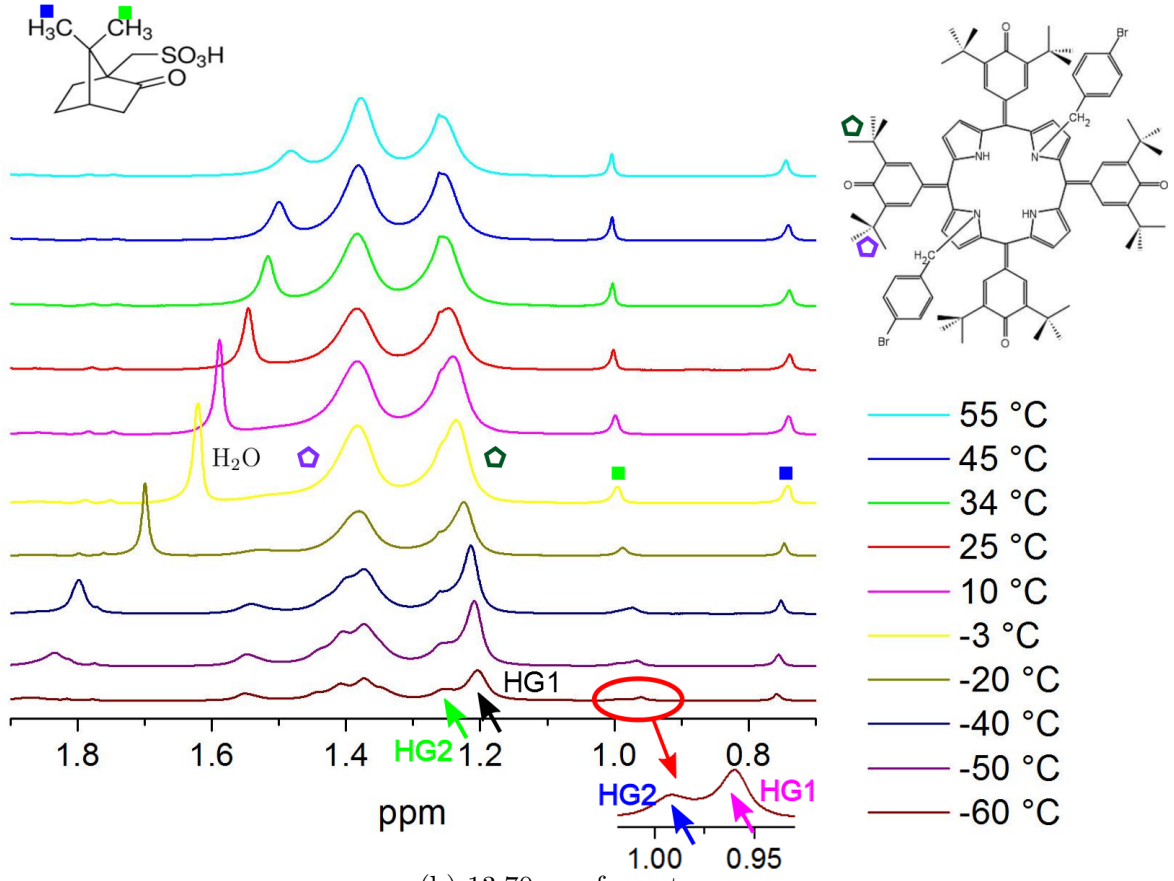

(b) 13.70 eq of guest

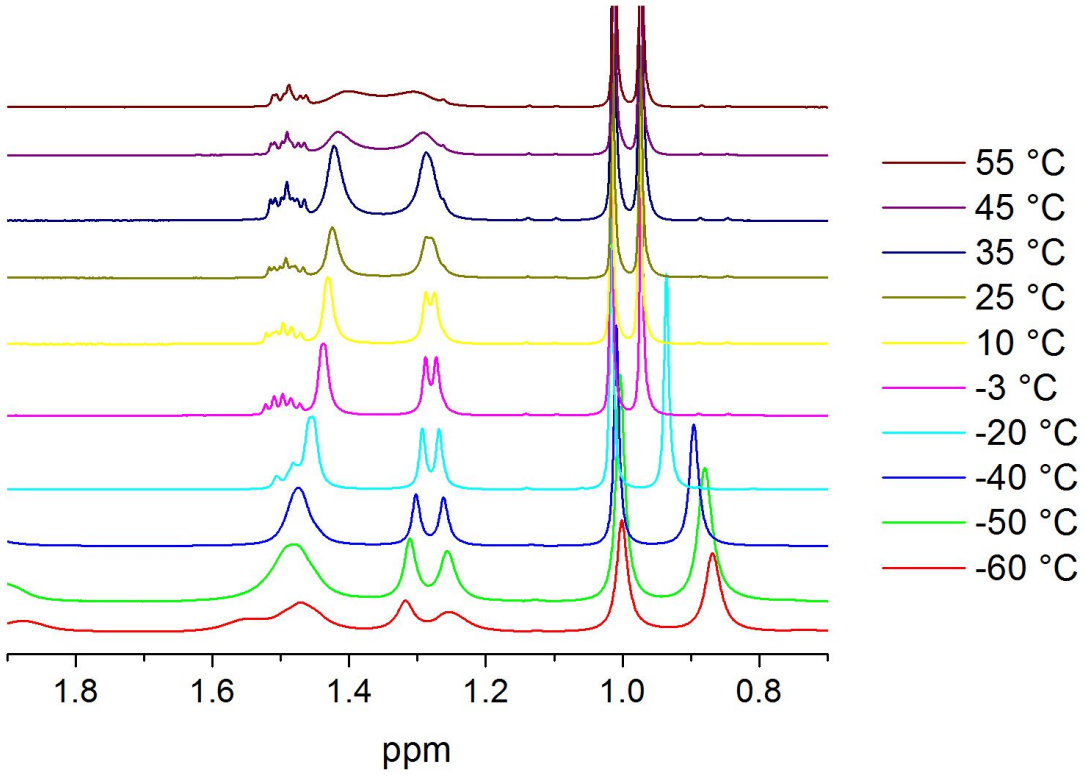

Figure 2.15: Variable temperature measurement of DiBrBzOxP with two different amount of (*R*)-camphorsulfonic acid.

(a) 0.54 eq of guest

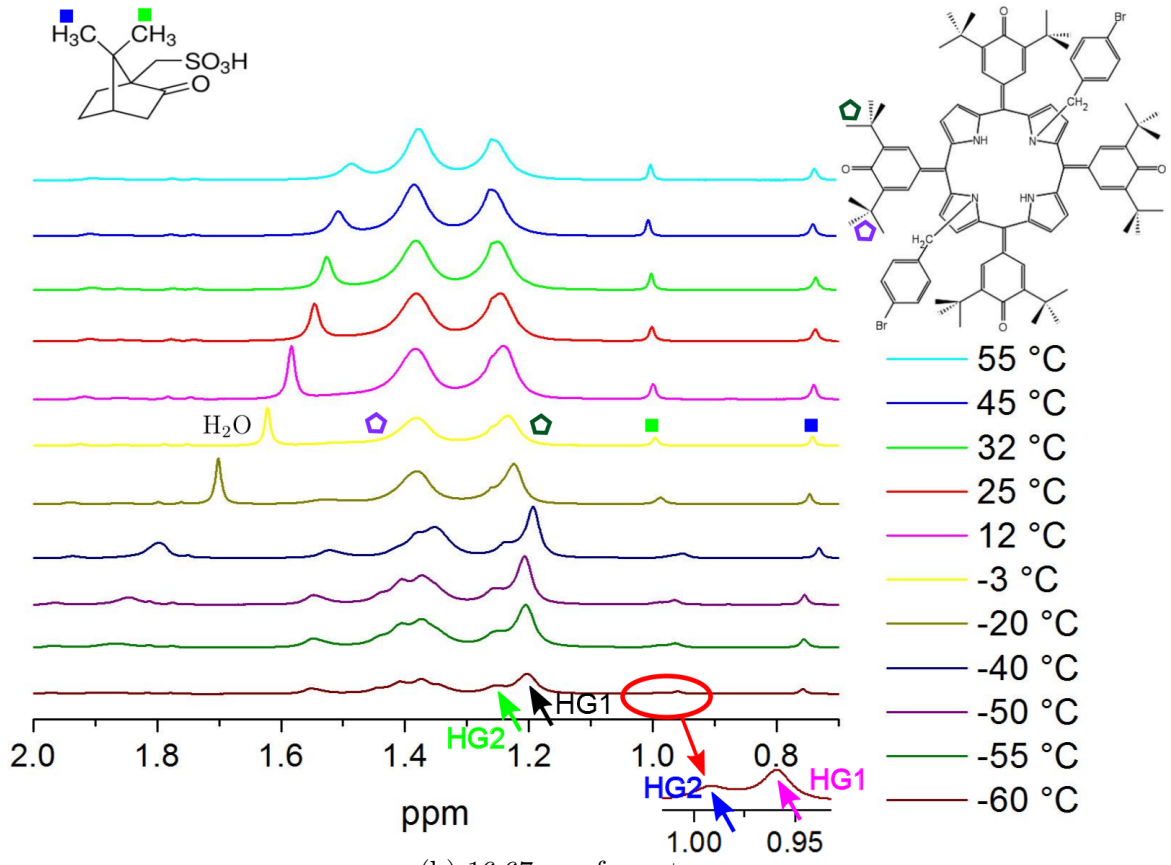

(b) 16.67 eq of guest

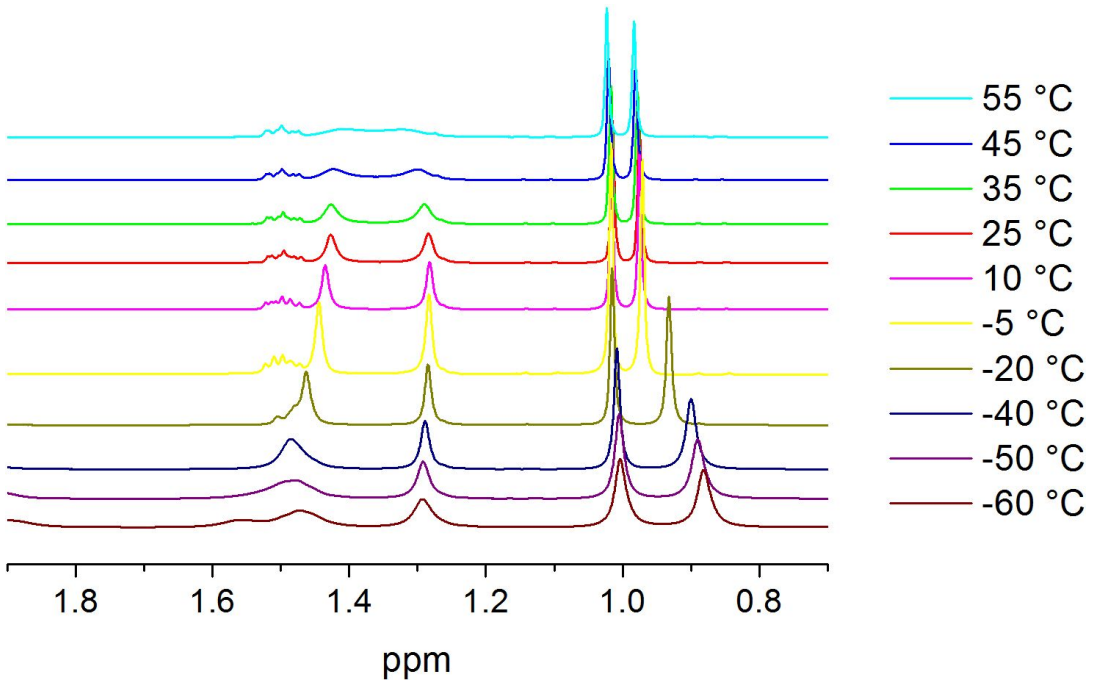

Figure 2.16: Variable temperature measurement of DiBrBzOxP with two different amount of racemic camphorsulfonic acid.

On the other hand both series of measurements (with (R)- and racemic form) for guest concentrations above 1 eq show considerable changes of guest methyl

group shifts. Guest molecules are under exchange between free and complexed state so this change in spectrum is given by temperature dependence of equilibrium constant $K_{\mathbf{HG}}$ and consequently by temperature dependence of free and complexed state populations.

Variable temperature effects on host *tert*-butyl peaks

Host *tert*-butyl signals show more information about complex. At first we consider spectra measured with guest concentration below 1 eq (Figures 2.15a and 2.16a). There is no difference between spectra of pure guest (*R*)-form and spectrum of racemic guest. Therefore, enantiomeric excess has negligible influence. We can see that with decreasing temperature *tert*-butyl peak at 1.2 ppm splits into two inequal peaks (green and black arrows in the Figures 2.15a and 2.16a) and the other *tert*-butyl peak at 1.4 ppm splits even to more peaks (maybe four peaks at 1.4 ppm and one at 1.55 ppm but they are very broad). We conclude that process responsible for this peak splitting is protonation of carbonyl groups. Their areas reveal populations 0.30:0.70. The ratio is almost the same like for the guest. However, resonances for host are a bit altered because of presence of non-protonated species.

Splitting of *tert*-butyl groups indicates that there are at least two conformations of protonated state on host-guest complex. (See QM computations in the next chapter.).

Now let us look at the other two series of spectra measured for high guest concentration (Figures 2.15b and 2.16b). At low temperatures *tert*-butyl signal at 1.3 ppm in spectra with $\mathbf{G}_R$ shows splitting which is invisible at room temperature. But this splitting is missing in spectra with racemic guest. So it is unambiguously the same effect of chirality transfer we have seen on β-protons in the Figure 2.13.

The last effect observable from *tert*-butyl signals is significant broadening of the both *tert*-butyl peaks which is observable at high temperatures and at high guest concentration (See spectra at 45 and 55 °C in the Figures 2.15b and 2.16b.). It is caused by chemical exchange and it implies rotation of the whole protonated group bound to *meso*-carbon (Figure 2.17, denoted with blue color). Upon

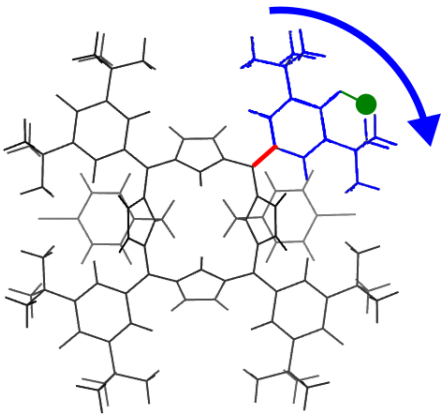

Figure 2.17: Rotation of hydroxyphenyl group.

protonation the whole oxo-cyclohexadienylidene group becomes hydroxyphenyl

group bound to the *meso*-carbon with the single bond (denoted red in the Figure 2.17).

However, at guest concentrations below 1 eq this process does not significantly influence the spectrum because exchange of protonation at carbonyl groups is slow. Therefore only 1/4 of the whole signal of *tert*-butyl groups broadens. At higher guest concentrations the protonation exchanges fast thus in average all carbonyl groups are protonated and so all four hydroxyphenyl groups rotate at the NMR time scale.

Variable temperature effects on NH resonances

Now we focus on downfield area of spectra with NH resonances. Measurements with higher concentrations of guest reveal no interesting behavior. In both racemic and enantiopure mixture there is only one NH signal from complexed porphyrin at 12.3 ppm because of the regime of fast exchange (e.g. Figure 2.3, high concentrations). Its chemical shift remains constant over the whole range of temperatures.

However, dynamics of complex has influence on spectra measured for low guest concentrations (under 1 eq, Figure 2.18). Both racemic and enantiopure mixture

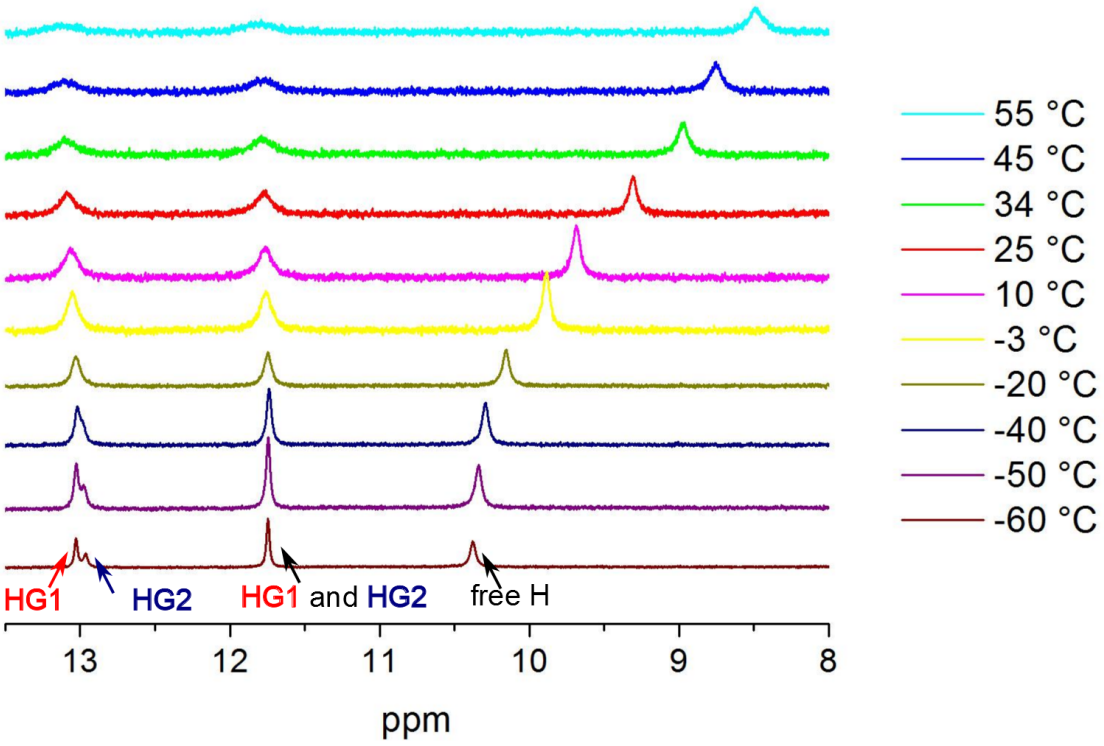

Figure 2.18: Variable temperature measurement of DiBrBzOxP in presence of 0.59 eq of (*R*)-camphorsulfonic acid.

of host and guest show the same behavior so *ee* has no influence on NH resonances. Spectra of **H** in presence of $\mathbf{G}_R$ as detected at various temperatures are depicted in the Figure 2.18. These spectra contain three NH resonances: moving resonance of free porphyrin and two resonances of complexed porphyrin at 11.7 and 13.0 ppm that do not change their position with temperature. At high temperatures signals of complex broaden because they are near coalescence. At

low temperatures peak at 13.0 ppm splits into two inequal peaks (red and blue arrows in the Figure 2.18). Both of these resonances originate from two different conformations of the complex, we denote them HG1 and HG2. From areas of the NH peaks we obtained the populations (HG1):(HG2):(free **H**) 0.27:0.43:0.30. Relative population of complexed species are almost the same as we have identified from guest methyl and host *tert*-butyl peaks. See comparison in the Table 2.1 (population from host *tert*-butyl peaks is less reliable).

Table 2.1: Comparison of experimental values of population of particular conformations of host-guest complex. Values denoted with * are less reliable.

	guest methyl peak [%]	host *tert*-butyl peak [%]	host NH peak [%]
HG1	65	70*	74
HG2	35	30*	26

Detailed discussion about geometry of possible conformations will be introduced in the next chapter.

2.2 Quantum chemistry computations

NMR is a powerful instrument suitable for investigating details about host-guest complexation. But NMR cannot determine the exact geometry of complex. For this purpose quantum chemistry computations are very useful. By this way we can compute conformations with the lowest energy, their population and even NMR shifts that can be compared to experimental values.

2.2.1 Methods

The investigated system of host-guest complex consists of 233 atoms and 996 electrons. This is quiet large system where we cannot use the most sophisticated and demanding methods because of limited computational capacity. But still Density functional theory (DFT) methods combined with relatively smaller basis 3-21G* provide solid instrument for exploring this complex. All computations were performed with the programme Gaussian [16]. For better modelling of disperse forces between complexed molecules we used D3 version of Grimme's dispersion with Becke - Johnson damping (Gaussian keyword `GD3BJ`) [18]. All computations included influence of solvent through Gaussian default polarized continuum model (PCM). The investigated molecule is placed to the continuum environment with electric permitivity of given solvent which simulates averaged interactions with solvent molecules [20], [21]. We also used density fitting approximation [19] for accelerating computing of Coulomb interaction. Automatically generated density fitting set was used (Gaussian keyword `auto`).

2.2.2 Possible conformations

At first we performed geometry optimizations at BLYP/3-21G* level. Usage of empirical dispersion proved to be very important for convergence of self-consistent field energy computations of complex. Plot of the electrostatic potential surfaces of deprotonated and protonated form of host molecule is in the Figures 2.19a and 2.19b. Blue color implies low energy for a negative charge. From electrostatic po-

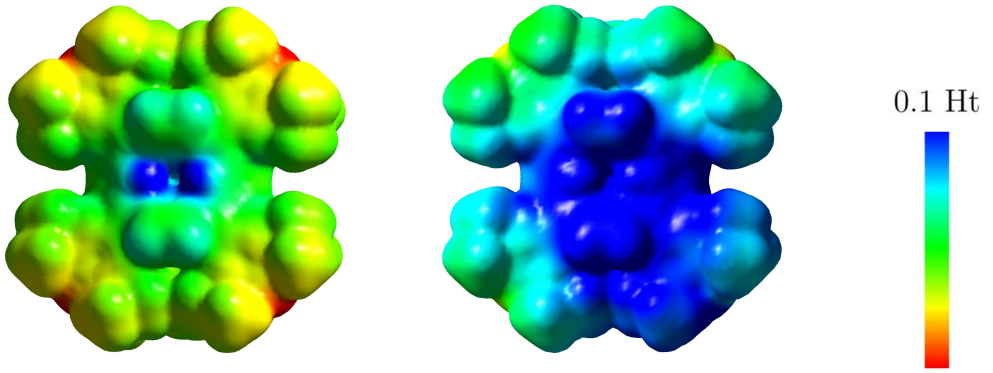

(a) DiBrBzOxP (b) protonated DiBrBzOxP

Figure 2.19: Electrostatic potential surface of two species of DiBrBzOxP (without guest) at electron density 0.001 e/a_B^3 computed at BLYP/3-21G* level ($1Ht = 627.51$ kcal/mol). Molecules are viewed from their site with NH groups. Protonation in the Figure (b) occurs at the right bottom corner of molecule.

tential surface can be seen that protonation of host significantly increases affinity for negatively charged molecules. We explored possible conformations for all four combinations of free or protonated host and free or deprotonated guest and compared their energies. However, the lowest energies were observed in complexes of protonated host and deprotonated guest. Unfortunately vibrational analysis revealed imaginary frequencies. This system is quiet large and the used method did not allow simply reach the minimum. Unbalanced entropic contribution of imaginary frequencies did not allow reliably determine the ΔG of association. Thus populations of found conformations (equation 1.23) were computed using ΔE (difference of electronic ground state energies) instead of ΔG. Finally we sorted out only two nonnegligibly populated conformations (denoted HGI and HGII, depicted in the Figures 2.20a and 2.20b) which have corresponding placement of guest but they differ in place of host protonation. Finding of two stable conformations and their population are in agreement with low temperature experiments[9] (Table 2.2). The most favourable position for guest negative charged SO_3 group is in the middle of tetrapyrrole macrocycle. Because of oxygen electronegativity partial negative charge arises at guest carbonyl group and it tends to move between two oxo-cyclohexadienylidene groups one of which is protonated.

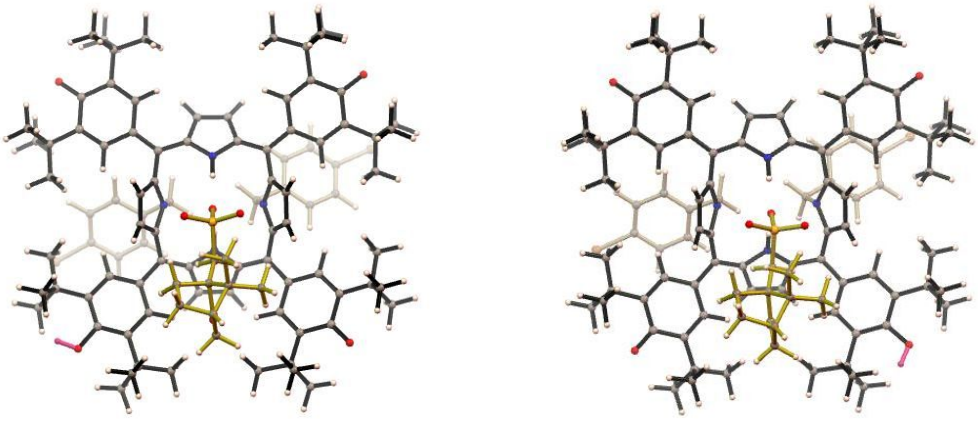

(a) HGI (b) HGII

Figure 2.20: Two most populated complex conformations, geometry and energy obtained at BLYP/3-21G* level. Guest molecule is yellow, protonation of host molecule is denoted by magenta color.

[9]However, we have no experimental evidence of right assignment of experimental populations to the particular computed conformations.

Table 2.2: Relative protonated conformations at −60 °C computed at the BLYP/3-21G* level compared to ^{1}H NMR experimental values Values denoted with * are less reliable.

	energy [kcal/mol]	computed population [%]	experimental: guest methyl peak [%]	experimental: host NH peak [%]	experimental: host *tert*-butyl peak [%]
HGI	-87.2	79	65	74	70*
HGII	-86.7	21	35	26	30*

Computing of NMR shifts

Geometries of conformations cannot be confirmed directly, however, quantum chemistry allows computation of chemical shifts that are directly comparable with NMR measurements. Used method for computing chemical shifts reads gauge-independent atomic orbital method (GIAO, [22], [23]). For this type of computations better functionals and bigger basis are neccessary - density of core electrons should be precisely modeled. After making a benchmark of a few functionals and a few sizes of basis we have chose the method PBE1PBE/6-31G(2df,2pd) (without the density fitting approximation) using GD3BJ empirical dispersion. We realized adding more polarization functions has positive effect on accuracy. However, geometry optimization at this level would take enormous amount of time so we made only single point computations at the already computed BLYP/3-21G* geometry. This practice is widely used approximation (see e.g. [17]). Attempts using better BLYP/6-31G(d,p) geometry give results of similar accuracy.

As we have seen in the experimental part ^{1}H NMR spectra are influenced by chemical exchange with guest and even with water[10]. Therefore we should be careful on choosing the proper experimental value to be compared with computations. At first we computed chemical shifts of pure host and guest. Considering guest molecule, there are only four well distinguished peaks originating from: both methyl groups at 1.00 and 1.03 ppm, two methylene protons at 3.13 and 3.45 ppm[11] and one broad peak from OH group (Figure 2.2). However, shift of the OH group is influenced by chemical exchange with water and can not be used for comparison with computations. Calculated shifts of three protons of corresponding methyl group were averaged because all three rotation states have equal energy.

Table 2.3: Computation of chemical shifts of chosen protons of camphorsulfonic acid by GIAO/PBE1PBE/6-31G(2df,2dp)/PCM method. Chemical shifts are in [ppm] unit.

	methyl 1	methyl 2	methylene 1	methylene 2
experiment	1.00	1.02	3.13	3.45
computation	0.92	1.34	3.44	3.45

[10]However, only shift of NH peak is significantly influenced by presence of water [13].

[11]In the spectrum we see four peaks that correspond to AB system. This peaks were fitted with the equations 1.13, 1.14 and 1.15 and two actual shifts were obtained.

Considering host molecule, experimental shifts of all peaks were usable for comparison with computations except the exchanging NH peak and the meta-brombenzyl proton peak which overlaps with solvent (Figure 2.1). In [13] titration of DiBrBzOxP with water was performed and NH shift 7.86 ppm was obtained after extrapolation to zero water concentration. Computed shifts are in the Table 2.4.

Table 2.4: Computation of chemical shifts of chosen protons of DiBrBzOxP by GIAO/PBE1PBE/6-31G(2df,2dp)/PCM method. Chemical shifts are in [ppm] unit.

	β ■	o-cyclohexadien ●	*tert*-butyl 1	methylene	NH
experiment	6.90	6.98	1.23	4.41	7.86
computation	7.65	6.97	1.27	4.42	8.52
	β ■	o-cyclohexadien ●	*tert*-butyl 2	*o*-brombenzyl ▲	
experiment	6.57	7.58	1.35	6.65	
computation	6.91	8.12	1.43	7.27	

In case of host-guest complex we chose experimental values of chemical shift of host β-protons (bound to alkylated pyrrole, ■ in the Figure 2.4) and guest methyl groups for comparison with computations. In calculations chiral guest molecule induces different chemical shifts (δ_A, δ_B, δ_C and δ_D) at all four investigated β-protons (see Figure 2.21). However, if only host and enantiopure guest are present in the sample, due to averaging by chemical exchange only two peaks are in the spectrum (■ in the Figure 2.4). Because of C_{2v} symmetry of host[12] and no symmetry of guest the observed chemical shifts are $\delta_{obs\,1} = (\delta_A + \delta_D)/2$ (denoted by red color in the Figure 2.21) and $\delta_{obs\,2} = (\delta_B + \delta_C)/2$ (denoted by blue color in the Figure 2.21). According to this principle we compared the computed chemical

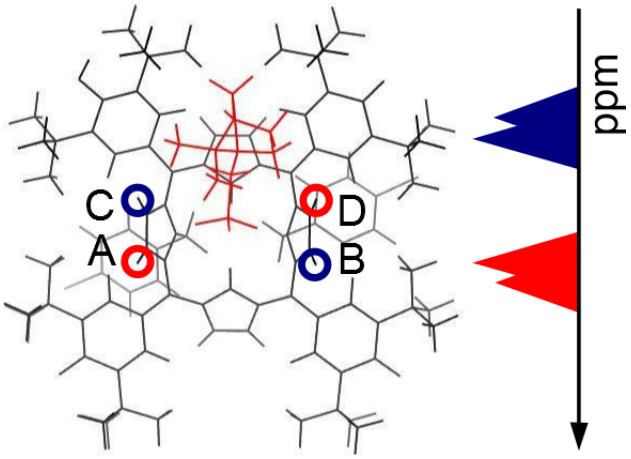

Figure 2.21: Averaging of β-protons chemical shifts due to chemical exchange of guest molecules.

shifts of particular conformations with experiment (first two rows in Table 2.5).

[12]Protonation does not disturb host symmetry when the protonation is in fast exchange regime (for high guest concentrations).

However, additional averaging over conformations is needed (third row in the Table 2.5).

Another peaks usable for comparison with computations are two guest methyl groups. Their chemical shift is influenced mainly by forming 1:1 host-guest com-

Table 2.5: Computation of chemical shifts of chosen protons of host-guest complex by GIAO/PBE1PBE/6-31G(2df,2dp)/PCM method. In the last row are shifts weighted with population (HGI):(HGII) 0.79:0.21. Chemical shifts are in [ppm] unit.

	guest methyl 1	guest methyl 2	host β 1 (■)	host β 2 (■)
experiment	0.73	1.00	6.91	6.94
HGI	0.37	1.08	6.73	6.90
HGII	0.21	1.05	6.71	6.92
weighted	0.34	1.07	6.72	6.90

plexes. Fitting of dependence of their observed chemical shifts on guest concentration (Figure 2.8) revealed their actual chemical shifts in host-guest complex 1.00 and 0.73 ppm. Comparison of computed and experimental host-guest complex chemical shifts is in the Table 2.5. Calculated values correspond well with the experimental values. The main source of error is that we compute chemical shifts in one static conformation (at -273.15 °C) while we measure averaged values of dynamic processes (at -60 °C). Another source of error is usage of geometry computed with relative small basis.

2.3 Relation between host protonation and formation of host-guest complex

As we noted in section devoted to titration experiments there is an ostensible discrepancy when we have seen fast exchange at guest methyl peaks (no visible splitting) and slow exchange at host NH peaks (significant splitting). However, QM computations elucidated this problem, see Figure 2.22. Guest is bound to host at the two symmetrically placed (because of C_{2v} symmetry of host molecule) most energetically favourable sites. However, computed values imply that guest

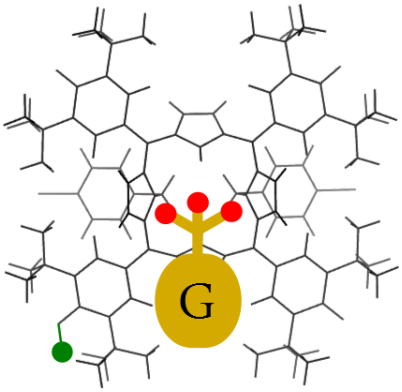

(a) probable
($\Delta E = -87.2$ kcal/mol, population 79%)

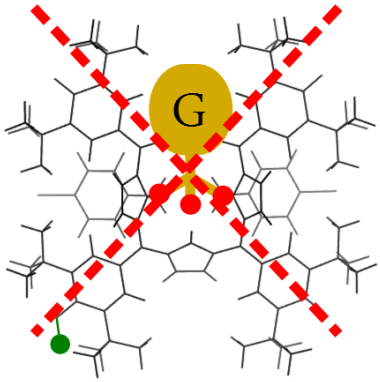

(b) improbable
($\Delta E = -83.5$ kcal/mol, population 0.01%)

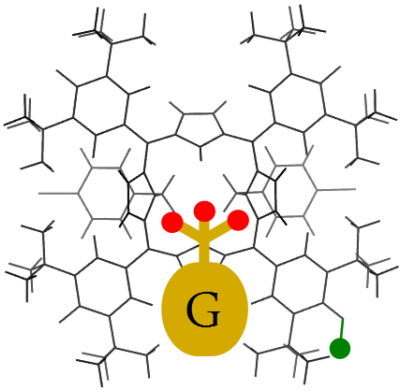

(c) probable
($\Delta E = -86.7$ kcal/mol, population 21%)

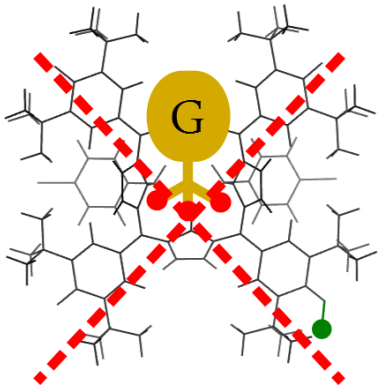

(d) improbable
($\Delta E = -82.7$ kcal/mol, population 0.002%)

Figure 2.22: Illustration of relation between protonation of host and formation of complex. Interaction energies computed at the BLYP/3-21G* level for complex of **H** and $\mathbf{G}_R$, populations were computed from this energies using Boltzmann distribution at room temperature.

molecule almost always binds to the host binding site which is in vicinity of host's protonation (Figure 2.22).

The measurements reveal that exchange of the protonation within the host (in the Figure 2.22 between (a) and (c)) is slow at low temperature and low guest concentration, see Figure 2.15a −60 °C. Therefore, if host is protonated, guest can bind to it only by unique way (As shown in the Figure 2.22 only states (a) and (c) are populated because states (b) and (d) are energetically unfavourable.). Despite

of fast exchange of guests in host-guest complex the NH resonances remain split (Figure 2.18, resonances at 11.5 - 13 ppm.).

When excess of the guest concentration is used then protonation within one host can exchange fast thus all host's carbonyl sites are protonated in average in the NMR time scale. It causes that host becomes symmetrical, both binding sites for guest become equally energetically favourable (Figure 2.23) and thus both NH resonances of complexed host become undistinguishable (see titration spectra in the Figure 2.3, spectra at guest concentration higher than 2 eq).

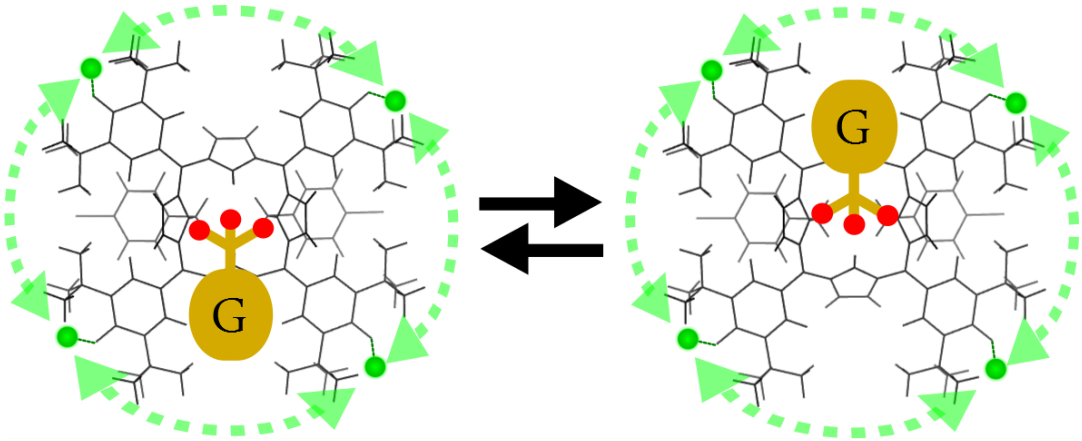

Figure 2.23: Illustration: both host binding sites for guest become equally energetically favourable if protonation of host is in fast exchange regime (at high concentrations of guest).

Chapter 3

Conclusion

NMR methods were used to investigate complex of porphyrin derivative with small chiral organic molecule. Besides spectroscopic methods the complex was also studied from a computational perspective to better understand the physical aspects of complex formation, host-guest interactions and transfer of guest chirality.

NMR titration experiments confirmed formation of host-guest complex of DiBrBzOxP and camphorsulfonic acid in 1:1 stoichiometry. Two titration experiments revealed association constant $K_{\mathbf{HG}} = 5.5 \times 10^4$ l/mol for (*R*)-form and $K_{\mathbf{HG}} = 4.7 \times 10^4$ l/mol for racemic form of guest. This values were compared to the value determinated by UV-vis titration $K_{\mathbf{HG}} = 1.07 \times 10^5$ l/mol. They differ by factor of two.

It was confirmed that splitting of host β-protons at alkylated pyrrole is sensitive to *ee* and its linear dependence was proved (Figure 2.14). Another signal whose splitting was sensitive to *ee* was one of the *tert*-butyl peaks (with lower chemical shift). However, it splits significantly only below 0 °C (Figure 2.15b).

We know from UV-vis titration that exactly one carbonyl group of DiBrBzOxP in presence of camphorsulfonic acid is protonated. Low temperature NMR measurements revealed two conformations which correspond to two different protonated forms of complex with populations around 0.7:0.3 (at −60 °C). Existence of two conformations was confirmed by QM computations which revealed population 0.79:0.21.

Chemical shifts of pure host, guest and host-guest complex were computed. Obtained values correspond to the measured values.

Host-guest complexation and its relation to protonation of host reveals two interesting effects. First, the guest prefers to bind to the binding site in the vicinity of host's protonated carbonyl.

Change in position of protonation of host's carbonyl group is slow at low guest concentrations (and fast at high guest concentrations) despite the fast exchange of guest molecules at host's binding site. Another interesting effect consists in rotation of the whole hydroxyphenyl group upon protonation of its carbonyl which can be considered as molecular rotor (Figure 2.17).

References

[1] Günter, H., NMR Spectroscopy: Basic Principles, Concepts, and Applications in Chemistry, *J*ohn Wiley and Sons, Chichester, 1995.

[2] Sanders, J. K. M., Hunter, B. K., Modern NMR Spectroscopy, *O*xford University Press Inc., New York, 1993.

[3] McQuarrie D. A., Simon J. D., Physical Chemistry: A Molecular Approach, *University Science Books,* USA, 1997.

[4] Piela, L., Ideas of Quantum Chemistry, *Elsevier*, Amsterdam, 2007.

[5] IUPAC-IUB Joint Commission on Biochemical Nomenclature (JCBN), Nomenclature of tetrapyrroles, *Eur. J. Biochem.,* 1988, 178, 277-328.

[6] Hill, J. P., Schmitt, W., McCarty, A. L., Ariga, K., D'Souza, F., Structures,Spectral and Electrochemical Properties of N-(Naphth-2-ylmethyl)-Appended Porphyrinogens, *Eur. J. Org. Chem.,* 2005, 2893-2902.

[7] Hill, J. P., Schumacher, A. L., D'Souza, F., Labuta, J., Redshaw, C., Elsegood, M. R. J., Aoyagi, M., Nakanishi, T., Ariga, K., Chromogenic Indicator for Anion Reporting Based on an N-Substituted Oxoporphyrinogen, *Inorg. Chem.,* 2006, 8288-9206.

[8] Isihara, S., Labuta, J., Sikorsky, T., Burda, J. V., Okamoto, N., Abe, H., Ariga, K., Hill, J. P., Colorimetric detection of trace wter in tetrahydrofuran using N,N'-substituted oxoporphyrinogens, *Chem. Commun.,* 2012, 3933-3935.

[9] Labuta, J., Futera, Z., Isihara, S., Kourilova, H., Tateyama, Y., Ariga, K., Hill, J. P., Chiral Guest Binding as a Probe of Macrocycle Dynamics and Tautomerism in a Conjugated Tetrapyrrole, *J. Am. Chem. Soc.,* 2014, 136, 2112-2118.

[10] Parker, D., NMR Determination of Enantiomeric Purity, *Chem. Rev.,* 1991, 91, 1441-1457.

[11] Shundo, A., Labuta, J., Hill, J. P., Isihara, S., Ariga, K., Nuclear Magnetic Resonance Signaling of Molecular Chiral Information Using an Achiral Reagent, *J. Am. Chem. Soc.,* 2009, 131, 9494-9495.

[12] Labuta, J., Isihara, S., Shundo, A., Arai, S., Takeoka, S., Ariga, K., Hill, J. P., Chirality Sensing by Nonchiral Porphines, *Chem. Eur. J.,* 2011, 17, 3558-3561.

[13] Labuta, J., Isihara, S., Sikorsky, T., Futera, Z., Shundo, A., Hanykova, L., Burda, J. V., Ariga, K., Hill, J. P., NMR spectroscopic detection of chirality and enantiopurity in referenced systems without formation of diastereomers, *Nat. Commun.* 2013, 4, 2188.

[14] Labuta, J., Ishihara, S., Ariga, K., Hill, J., Dynamic processes in Prochiral Solvating Agents (pro-CSAs) studied by NMR Spectroscopy *Symmetry,* in press.

[15] Sikorski, T., Study of chiral properties of supramolecular complexes, diploma thesis, *Charles University in Prague, Faculty of Mathematics and Physics,* 2011.

[16] Frisch, M. J. , Trucks, G. W., Schlegel, H. B., Scuseria, G. E., Robb, M. A., Cheeseman, J. R., Scalmani, G., Barone, V., Mennucci, B., Petersson, G. A., Nakatsuji, H., Caricato, M., Li, X., Hratchian, H. P., Izmaylov, A. F., Bloino, J., Zheng, G., Sonnenberg, J. L., Hada, M., Ehara, M., Toyota, K., Fukuda, R., Hasegawa, J., Ishida, M., Nakajima, T., Honda, Y., Kitao, O., Nakai, H., Vreven, T., Montgomery, J. A. Jr., Peralta, J. E., Ogliaro, F., Bearpark, M., Heyd, J. J., Brothers, E., Kudin, K. N., Staroverov, V. N., Keith, T., Kobayashi, R., Normand, J., Raghavachari, K., Rendell, A., Burant, J. C., Iyengar, S. S., Tomasi, J., Cossi, M., Rega, N., Millam, J. M., Klene, M., Knox, J. E., Cross, J. B., Bakken, V., Adamo, C., Jaramillo, J., Gomperts, R., Stratmann, R. E., Yazyev, O., Austin, A. J., Cammi, R., Pomelli, C., Ochterski, J. W., Martin, R. L., Morokuma, K., Zakrzewski, V. G., Voth, G. A., Salvador, P., Dannenberg, J. J., Dapprich, S., Daniels, A. D., Farkas, O., Foresman, J. B., Ortiz, J. V., Cioslowski, J., Fox, D. J., Gaussian 09, Revision D.01, *Gaussian, Inc.*, Wallingford CT, 2013.

[17] Foresman, J. B., Frisch, A., Exploring Chemistry with Electronic Structure Methods, 2nd edition, *Gaussian, Inc.,* Pittsburgh, 1996.

[18] Grimme, S., Ehrlich, S., Goerigk, L., Effect of the damping function in dispersion corrected density functional theory, *J. Comp. Chem.* 2011, 32, 1456-65.

[19] Dunlap, B. I., Fitting the Coulomb Potential Variationally in X-Alpha Molecular Calculations, *J. Chem. Phys.,* 1983, 78, 3140-42.

[20] Scalmani, G., Frisch, M. J., Continuous surface charge polarizable continuum models of solvation. I. General formalism, *J. Chem. Phys.,* 2010, 132, 114110.

[21] Tomasi, J., Mennucci, B., Cammi, R., Quantum mechanical continuum solvation models, *Chem. Rev.,* 2005, 105, 2999-3093.

[22] Wolinski, K. , Hilton, J. F. , Pulay, P. , Efficient Implementation of the Gauge-Independent Atomic Orbital Method for NMR Chemical Shift Calculations, *J. Am. Chem. Soc.,* 1990 112, 8251-60.

[23] Cheeseman, J. R. , Trucks, G. W. , Keith, T. A. , Frisch, M. J. , A Comparison of Models for Calculating Nuclear Magnetic Resonance Shielding Tensors, *J. Chem. Phys.,* 1996, 104, 5497-509.